

Machine learning-aided engineering of hydrolases for PET depolymerization

<https://doi.org/10.1038/s41586-022-04599-z>

Received: 10 October 2021

Accepted: 28 February 2022

Published online: 27 April 2022

 Check for updates

Hongyuan Lu¹, Daniel J. Diaz², Natalie J. Czarnecki¹, Congzhi Zhu¹, Wantae Kim¹, Raghav Shroff^{3,4}, Daniel J. Acosta³, Bradley R. Alexander³, Hannah O. Cole^{1,3}, Yan Zhang³, Nathaniel A. Lynd¹, Andrew D. Ellington³ & Hal S. Alper^{1,✉}

Plastic waste poses an ecological challenge^{1–3} and enzymatic degradation offers one, potentially green and scalable, route for polyesters waste recycling⁴. Poly(ethylene terephthalate) (PET) accounts for 12% of global solid waste⁵, and a circular carbon economy for PET is theoretically attainable through rapid enzymatic depolymerization followed by repolymerization or conversion/valorization into other products^{6–10}. Application of PET hydrolases, however, has been hampered by their lack of robustness to pH and temperature ranges, slow reaction rates and inability to directly use untreated postconsumer plastics¹¹. Here, we use a structure-based, machine learning algorithm to engineer a robust and active PET hydrolase. Our mutant and scaffold combination (FAST-PETase: functional, active, stable and tolerant PETase) contains five mutations compared to wild-type PETase (N233K/R224Q/S121E from prediction and D186H/R280A from scaffold) and shows superior PET-hydrolytic activity relative to both wild-type and engineered alternatives¹² between 30 and 50 °C and a range of pH levels. We demonstrate that untreated, postconsumer-PET from 51 different thermoformed products can all be almost completely degraded by FAST-PETase in 1 week. FAST-PETase can also depolymerize untreated, amorphous portions of a commercial water bottle and an entire thermally pretreated water bottle at 50 °C. Finally, we demonstrate a closed-loop PET recycling process by using FAST-PETase and resynthesizing PET from the recovered monomers. Collectively, our results demonstrate a viable route for enzymatic plastic recycling at the industrial scale.

Enzymatic depolymerization of PET was first reported in 2005 and has been nascently demonstrated using 19 distinct PET-hydrolysing enzymes (PHEs) derived from esterases, lipases and cutinases^{4,11,13}. However, most of these enzymes only show appreciable hydrolytic activity at high reaction temperatures (that is, at or exceeding the PET glass transition temperature of roughly 70 °C) and with highly processed substrates. For example, an engineered leaf-branch compost cutinase (LCC) can degrade 90% of pretreated postconsumer-PET (pc-PET) in 10 h at 72 °C and a pH of 8.0 (ref. ¹²). Most other PHEs similarly show poor activity at moderate temperatures¹⁴ and more neutral pH conditions¹⁵, greatly restricting in situ/microbially enabled degradation solutions for PET waste. This limitation is of critical concern as 40% of plastic waste bypasses collection systems and resides in natural environments¹⁶. In addition, converting untreated postconsumer plastic waste at near ambient temperatures would lower net operating costs.

Although the PHE from the PET-assimilating bacterium *Ideonella sakaiensis*¹⁴ (PETase) can operate at ambient conditions, it is highly labile and loses activity even at 37 °C after 24 h (ref. ¹⁷). Nonetheless, this mesophilic enzyme has previously seen attempts to enhance thermostability, robustness and function^{17–23}. The most notable engineered

PETase variants—ThermoPETase¹⁷ and DuraPETase²²—were created through rational protein engineering and computational redesign strategies, respectively. Although the thermostability and catalytic activity of these two mutants were improved^{17,22} under certain conditions, they nonetheless had overall lower PET-hydrolytic activity at mild temperatures.

We posited that highly focused protein engineering approaches cannot consider the evolutionary trade-off between overall stability and activity, and that a neutral, structure-based, deep learning neural network could generally improve enzyme function. To this end, we used a three-dimensional (3D) self-supervised, convolutional neural network (CNN), MutCompute²⁴ (<https://mutcompute.com>; Supplementary Fig. 1 and Supplementary Discussion) to identify stabilizing mutations. This algorithm learns the local chemical microenvironments of amino acids on the basis of training over 19,000 sequence-balanced protein structures from the Protein Data Bank (PDB) and can readily predict positions within a protein in which wild-type (WT) amino acids are not optimized for their local environments. We used MutCompute to obtain a discrete probability distribution for the structural fit of all 20 canonical amino acids at every position in both WT PETase and ThermoPETase (crystal

¹McKetta Department of Chemical Engineering, The University of Texas at Austin, Austin, TX, USA. ²Department of Chemistry, The University of Texas at Austin, Austin, TX, USA. ³Department of Molecular Biosciences, The University of Texas at Austin, Austin, TX, USA. ⁴DEVCOM ARL-South, Austin, TX, USA. [✉]e-mail: halper@che.utexas.edu

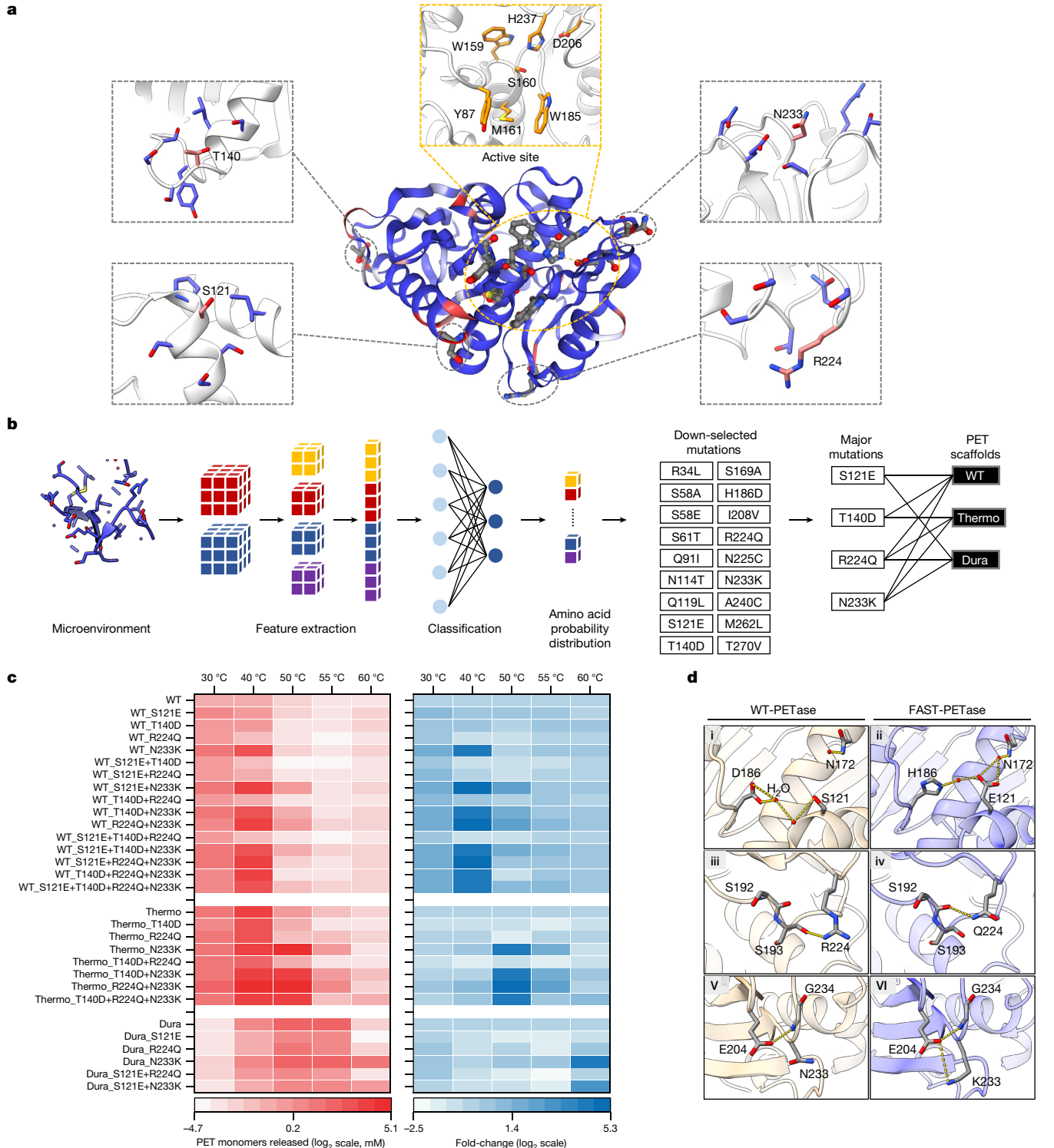


Fig. 1 | Machine learning guided predictions improve enzyme performance across PETases scaffolds. **a**, WT PETase protein structure rendered by the output of MutCompute. Each amino acid residue was assigned a probability distribution reflecting the chemical congruity (shown in red, disfavoured and blue, favoured) with the neighbouring chemical microenvironments. Local microenvironments near the active site and major disfavoured amino acid residues (S121, T140, R224, N233) are shown as magnified panels and highlighted as pink sticks. Active site residues are shown as orange sticks. **b**, Predictions based on both WT PETase and ThermoPETase were ranked by the fold change in the probabilities between the predicted and the WT amino acid. 159 variants were generated by incorporating single or several predicted mutations into various PETase scaffolds to result in four mutations (S121E, T140D, R224Q and N233K) with the highest improvements both singly and in combination. These mutations were combinatorially assembled

across three PETase scaffolds: WT PETase (WT), ThermoPETase (Thermo) and DuraPETase (Dura). **c**, The red heatmap (left) shows the PET-hydrolytic activity of the resulting variants and the blue heatmap (right) shows the fold change of activity over their respective scaffolds on the basis of total PET monomers (the sum of TPA and MHE) released from hydrolysing circular gf-PET film (6 mm in diameter, roughly 11.4 mg) by the PETase variants after 96 h of incubation at temperature ranging from 30 to 60 °C. All measurements were conducted in triplicate ($n=3$), and the mean values were used for generating the heatmaps. **d**, Predicted mutations from neural network algorithm stabilize FAST-PETase (I–VI). Structural comparison between (I, III, V) WT PETase (tan-coloured stick model, PDB code 5XJH) and (II, IV, VI) FAST-PETase (blue-coloured stick model, PDB code 7SH6) near the predicted mutation sites (S121E, R224Q, N233K, respectively). Hydrogen-bonding and salt bridge interactions are shown and highlighted as yellow dotted lines.

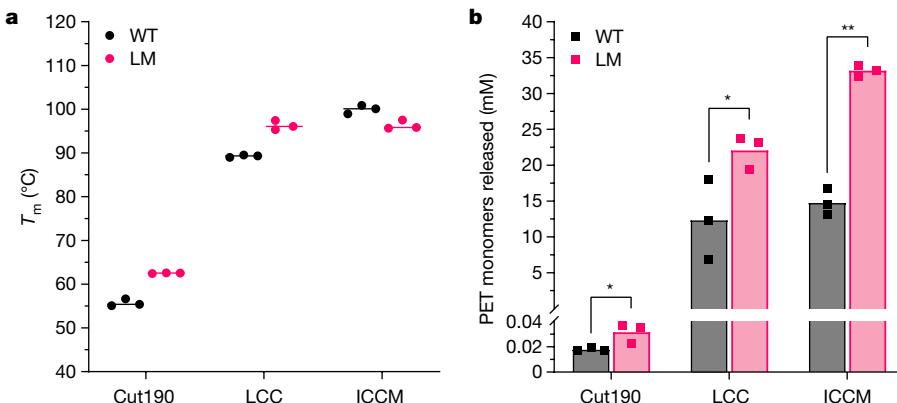


Fig. 2 | The thermostability and PET-hydrolytic activity of WT and lysine mutation enzymes. **a.**, T_m of WT and lysine mutation (LM) enzymes was determined by DSC. **b.**, PET-hydrolytic activity was evaluated by measuring the amount of PET monomers (the sum of TPA and MHET) released from hydrolysing amorphous gf-PET with WT and lysine mutation enzymes. The reaction temperatures for each group of enzymes were as follows: Cut190,

50 °C; LCC, 70 °C and ICCM, 70 °C. KH₂PO₄-NaOH (pH 8) buffer was used for all enzymes shown in this figure. All measurements were conducted in triplicate ($n = 3$). The bars and circles or squares shown for each enzyme represent the average and individual numbers, respectively. Statistical analyses using a one-sided *t*-test were performed to compare the PET monomers released by the WT and variant enzymes. * $P < 0.05$, ** $P < 0.0001$.

structures, PDB 5XJH and 6IJ6) (Supplementary Table 1), essentially carrying out an *in silico* comprehensive mutagenesis scan. The predicted distributions were rendered onto the protein crystal structure (Fig. 1a) to identify positions where WT amino acid residues fitted less well than potential substitutions. Predictions were then ranked by predicted probabilities (fold change of fit) (Fig. 1b, Extended Data Fig. 1 and Supplementary Table 2). Using a stepwise combination strategy, a total of 159 single or several predicted mutations were generated. Variants showing improved catalytic activity (as measured by esterase activity and plastic degradation rates) and thermostability (as measured by protein melting temperature, T_m) were characterized further. Among this set, four mutations (S121E, T140D, R224Q and N233K) (Fig. 1b) resulted in the highest improvements, both singly and in combination, and were selected for further assembly and analysis (see Supplementary Discussion for further discussion of mutant down-select).

We assembled all 29 possible combinations using these four mutations across three PETase scaffolds (WT PETase, ThermoPETase and DuraPETase). Of note, two could not be purified using the DuraPETase background after several attempts. Thermostability analysis of the remaining 27 mutants indicated that 23 (roughly 85%) resulted in elevated T_m relative to their respective scaffolds (Extended Data Fig. 2). The highest change in thermostability from their respective PETase scaffolds were observed for variants PETase^{T140D/N233K} with a T_m of 58.1 °C ($\Delta T_m = 10$ °C from WT PETase), ThermoPETase^{N233K} with a T_m of 67.2 °C ($\Delta T_m = 9$ °C from ThermoPETase) and DuraPETase^{N233K} with a T_m of 83.5 °C ($\Delta T_m = 5$ °C from DuraPETase). The last mutant represents the most thermostable PETase mutant reported so far. It was noted that the protein yield of all 27 variants was improved (up to 3.8-fold increase) compared with the parental scaffold, further underscoring the ability of MutCompute to identify mutants of higher stability.

Next, we sought to evaluate the PET-hydrolytic activity of these more stable variants across a range of temperatures from 30 to 60 °C using an amorphous PET film (gf-PET, from the supplier Goodfellow) commonly used in the literature¹². This comparison immediately revealed that the machine learning guided predictions greatly enhanced activity and extended the working temperature range across all scaffolds (Fig. 1c). In particular, PETase^{S121E/R224Q/N233K} demonstrated a 3.4- and 29-fold increase in PET-hydrolytic activity at 30 and 40 °C, respectively, over WT PETase (Fig. 1c) at these same temperatures. Enzyme mutants based on the ThermoPETase scaffold showed an extended range of working temperature (30–60 °C) and showed substantially higher activity than their counterparts. Within this set, the best variant (containing N233K and R224Q on top of S121E), named FAST-PETase (functional, active,

stable and tolerant PETase), showed 2.4- and 38-fold higher activity at 40 and 50 °C, respectively, compared to ThermoPETase alone (Fig. 1c). At 50 °C, FAST-PETase showed the highest overall degradation of all mutants and temperatures tested here releasing 33.8 mM of PET monomers (the sum of terephthalic acid (TPA) and mono-(2-hydroxyethyl) terephthalate (MHET)) in 96 h (Fig. 1c). The DuraPETase scaffold, in general, showed relatively low activity at mild temperatures (30–50 °C), but mutant-based improvements were realized at higher temperatures (55–60 °C) as demonstrated by the most thermostable PETase mutant- DuraPETase^{N233K} (Fig. 1c). To fully evaluate the catalytic resilience of mutant enzymes to environmental conditions, FAST-PETase (PETase^{S121E/D186H/R224Q/N233K/R280A}) was compared to previously reported WT and mutant PHEs including WT PETase, ThermoPETase, DuraPETase, LCC and the most active mutant LCC^{F243I/D238C/S283C/N246M} (ICCM)¹² using amorphous gf-PET across a range of pH (6.5–8.0) and temperatures (30–40 °C) (Supplementary Fig. 2). Across these conditions, FAST-PETase emerged as an excellent candidate for mild temperatures and moderate pH conditions characteristic of *in situ* PET degradation.

Crystal structure analysis of FAST-PETase (PDB 7SH6; Extended Data Fig. 3 and Extended Data Table 1) at 1.44 Å resolution explains the enhanced stability through newly formed, favourable residue interactions (Fig. 1d). The N233K mutation places a positively charged lysine next to E204 and establishes an intramolecular salt bridge (Fig. 1d(vi)). The side chain of R224, when mutated to glutamine, forms a hydrogen bond to the carbonyl group of S192 (Fig. 1d(iv)). Finally, the S121E mutation enables a new water-mediated hydrogen-bonding network with H186 and N172 (Fig. 1d(ii)).

Next, we sought to investigate the portability and generalizability of the machine learning-based predictions using alternative PHEs. To this end, we selected the N233K mutation and introduced this corresponding lysine mutation to LCC, ICCM and the cutinase-like enzyme, Cut190, from *Saccharomonospora viridis* AHK190 (ref. ²⁵) (Extended Data Fig. 4 and Supplementary Fig. 3). The resulting lysine mutation variants of Cut190 and LCC (LCC^{D238K} and Cut190^{D250K}) both showed substantially enhanced thermostability ($\Delta T_m = 7$ °C) relative to their respective scaffolds (Fig. 2a) whereas the lysine mutation variant of ICCM (ICCM^{C238K/C283S}) demonstrated a T_m of 96.3 °C, a decrease of 3.7 °C. More importantly, the hydrolytic activity of all three of these lysine mutation variants on amorphous gf-PET were notably higher than their respective scaffolds (Fig. 2b), thus showcasing mutations portability.

Beyond model plastic substrates, it is critical to demonstrate the performance of PETase enzymes on raw, untreated pc-PET. Notably, unlike the gf-PET used above and throughout the literature, there is no

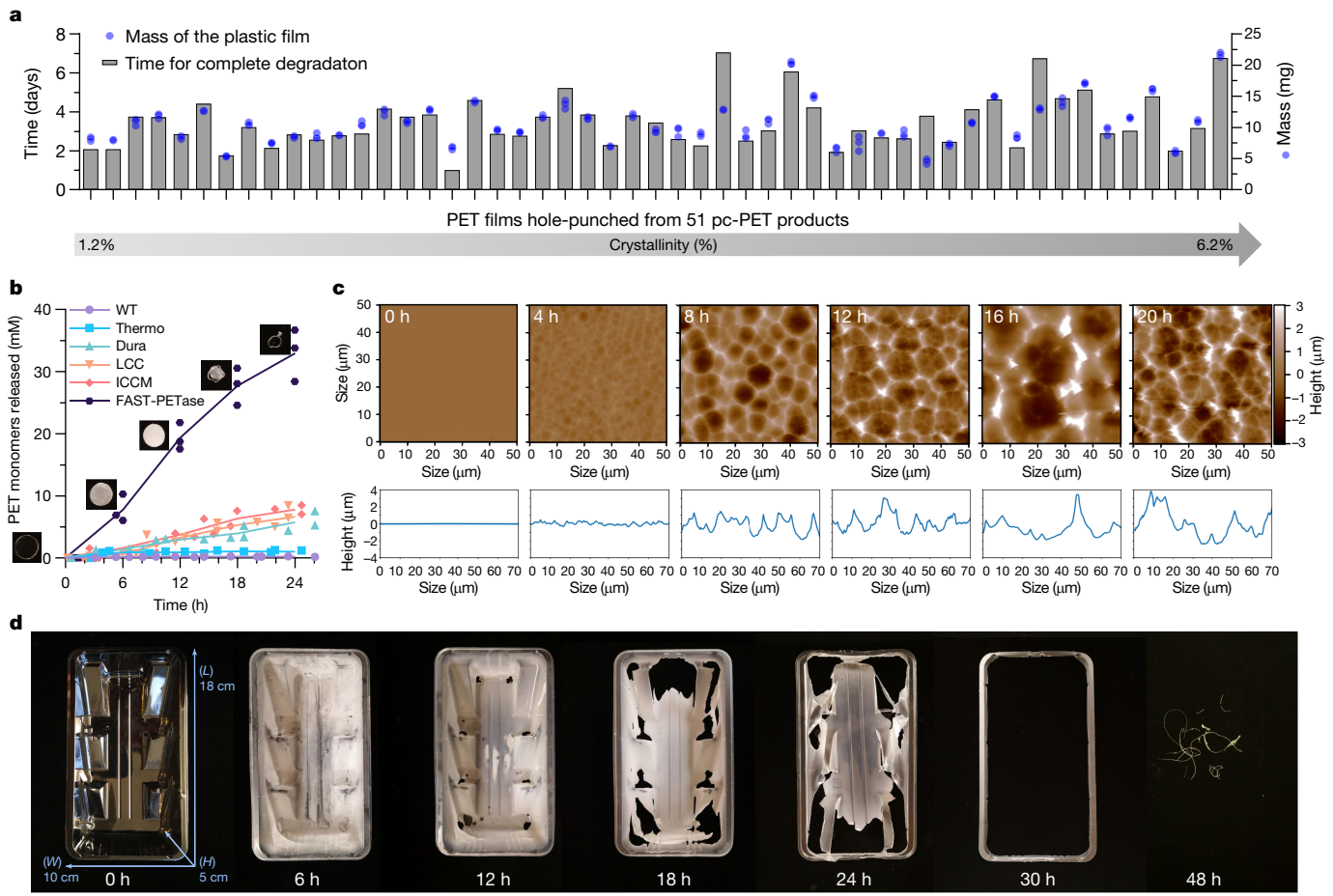


Fig. 3 | The superior performance of FAST-PETase in enzymatic depolymerization of thermoformed pc-PET products. **a**, Complete depolymerization of pc-PET films hole-punched from 51 postconsumer plastic products. **b**, Time course of PET-hydrolytic activity of FAST-PETase, WT PETase (WT), ThermoPETase (Thermo), DuraPETase (Dura), LCC and ICCM at reaction temperature of 50 °C. PET-hydrolytic activity was evaluated by measuring the amount of PET monomers (the sum of TPA and MHET) released from hydrolysing pc-PET (Bean cake plastic container) film by the tested PHEs at

various time points. $\text{KH}_2\text{PO}_4\text{-NaOH}$ (pH 8) buffer was used for all enzymes shown in this figure. All measurements were conducted in triplicate ($n = 3$). The line connects mean values of the timepoints. The symbols shown for each enzyme represent the individual numbers. **c**, AFM images of pc-PET films following various exposure times with FAST-PETase. **d**, Complete degradation of large, untreated PET container with FAST-PETase at 50 °C. *L*, length; *W*, width and *H*, height.

singular pc-PET substrate. To this end, we collected 51 samples of post-consumer plastic products used in the packaging of food, beverages, medications, office supplies, household goods and cosmetics available at local grocery store chains and treated this raw material enzymatically with FAST-PETase at 50 °C (Supplementary Table 3). Despite their heterogeneity across crystallinity, molecular weight, thickness and additives, hole-punched samples from this wide array of PET products were all fully degraded by FAST-PETase in 1 week and in as little as 24 h (Fig. 3a, Supplementary Table 3 and Supplementary Figs. 4 and 5). The depolymerization (as measured by monomers generation) by FAST-PETase occurred at an almost linear rate (Supplementary Fig. 4), accompanied by a corresponding linear mass loss of the films (Extended Data Fig. 5). Although degradation time did correlate with the thickness of the plastic (as thickness and mass are related) (Extended Data Fig. 6), no other singular, measured trait of these thermoformed, low crystalline PET determined degradation rates (Extended Data Fig. 7).

A time-course analysis (Fig. 3b) from a bean cake container revealed the almost linear decay rate and concomitant increase in crystallinity from 1.2 to 7.7% over 16 h (Supplementary Fig. 6). Atomic force microscopy (AFM) (Fig. 3c) as well as scanning electron microscopy (SEM) (Extended Data Fig. 8) further depict the reaction progression of FAST-PETase as it produced increasingly deeper and larger holes in

the pc-PET surface resulting in increased surface roughness (and visible opaqueness) over the course of the reaction (Supplementary Fig. 7). By contrast, the PET-hydrolytic activity of WT PETase, ThermoPETase, DuraPETase, LCC and ICCM towards this pc-PET was substantially lower (3.2- to 141.6-fold) than that of FAST-PETase under the same conditions (Fig. 3b). The activity of LCC and ICCM even at their previously reported optimal reaction temperature of 72 °C (ref. ¹²) was still 4.9- and 1.5-fold lower, respectively, than that of FAST-PETase at 50 °C. Further experimental analysis (Supplementary Fig. 8) indicated that LCC and ICCM showed their highest degradation rate against this pc-PET film at 60 °C, yet this activity was still lower than that of FAST-PETase at 50 °C. We also demonstrate that this FAST-PETase-enabled depolymerization is easily scalable to large, untreated pieces of plastic (in this case, 6.4 g rather than 11 mg) simply by increasing net reaction volumes (Fig. 3d).

We next sought to investigate whether commercial PET water bottles can be enzymatically hydrolysed by FAST-PETase. Different from the thermoformed postconsumer plastic products, water bottles are produced by blow-moulding, which makes most of the bottle highly crystalline (>25% crystallinity) resulting from the expansion process²⁶. Highly crystalline polymers are less susceptible to enzymatic attacks and even the growth of *L. sakaiensis* is restricted to low crystalline regions of water bottles²⁷. To more fully evaluate enzymatic depolymerization of

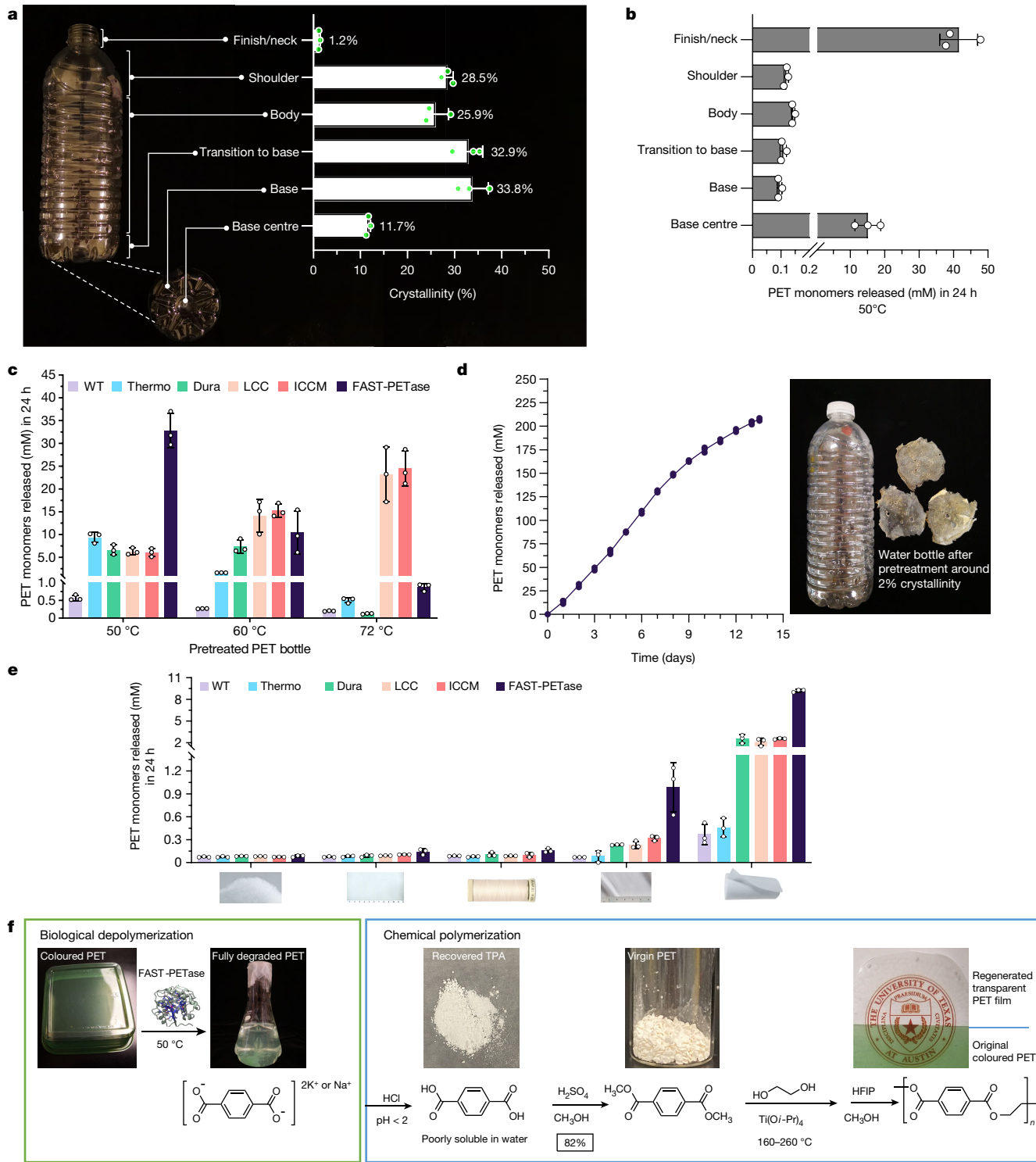


Fig. 4 | Depolymerization of PET water bottles and polyester products by FAST-PETase and application of FAST-PETase in enzymatic-chemical recycling of PET. **a**, Crystallinity (%) of top-to-bottom fragments of a PET water bottle (500 ml, CG Roxane LLC). **b**, Depolymerization of top-to-bottom fragments of a water bottle by FAST-PETase at 50 °C. **c**, PET monomers released from hydrolysing pretreated water bottle films (6 mm in diameter, roughly 25 mg) with FAST-PETase, WT PETase (WT), ThermoPETase (Thermo), DuraPETase (Dura), LCC and ICCM at reaction temperature ranging from 50 to 72 °C. **d**, Complete degradation of a pretreated water bottle (roughly 9 g) with FAST-PETase at 50 °C. 200 ml of fresh enzyme solution was replenished every 24 h to avoid product inhibition and maximize enzymatic depolymerization

rate. **e**, Depolymerization of five commercial polyester products (fibre fill, insulating fabric, thread, mosquito netting, batting) with various PHEs at 50 °C. **f**, Schematic of the closed-loop PET recycling process incorporating postconsumer coloured plastic waste depolymerization by FAST-PETase and chemical polymerization. The crystallinity of the regenerated PET was determined as 58% by DSC (Supplementary Fig. 12). The molecular weights (M_n , M_w), polydispersity indices (\bar{D}) of the regenerated PET were determined as $M_n = 16.4 \text{ kg mol}^{-1}$, $M_w = 45.9 \text{ kg mol}^{-1}$, $\bar{D} = 2.80$ by GPC. KH_2PO_4 -NaOH (pH 8) buffer was used for all enzymes shown in this figure. All measurements (**a-e**) were conducted in triplicate ($n = 3$). The bars and circles shown represent the average and individual numbers, respectively.

commercial water bottles, we determined the crystallinity of various sections of the bottle and find that the finish/neck and base centre are relatively amorphous (1.2 and 11.7% crystallinity) whereas the rest of the bottle is highly crystalline (25.9 to 33.8% crystallinity) (Fig. 4a). To evaluate biodegradability of raw, untreated sections of a water bottle, we cut out or hole-punched fragments from these regions and treated them with FAST-PETase at 50 °C for 24 h. Our results (Fig. 4b) show that substantial monomers release was achieved at the finish/neck and base centre region whereas only trace amounts of monomers (0.09 to 0.14 mM) were released for the rest of the bottle, thus indicating that high crystallinity negatively affects the enzymatic depolymerization rate.

PET polymer chains become more mobile and flexible at a temperature close to the glass transition temperature (roughly 70 °C)²⁸. Therefore, it has been proposed that conducting enzymatic depolymerization at higher temperatures could improve degradation susceptibility and rate²⁹. To investigate this hypothesis, we compared the hydrolytic activity of FAST-PETase with other PHEs, including the thermophilic enzymes LCC and ICCM across a range of temperatures from 50 to 72 °C. These results demonstrated that the highly crystalline body part still cannot be efficiently depolymerized by any tested enzymes and temperatures and that FAST-PETase at 50 °C exhibited the highest overall depolymerization rate (Extended Data Fig. 9). To tackle the challenge of complete water bottle degradation, we used a simple thermal pretreatment. By melting the whole bottle followed by a quick temperature quenching, the bottle PET became uniformly amorphous (roughly 2% crystallinity). By using hole-punched films from this pretreated bottle, we compared the hydrolytic activity of FAST-PETase along with other PHEs, across temperatures from 50 to 72 °C (Fig. 4c). These results indicate that FAST-PETase can efficiently depolymerize pretreated bottle films, releasing 32.8 mM of PET monomers at 50 °C in 24 h, which is the highest of among all PHEs and temperature combinations tested. At the same time, a slightly modified thermal pretreatment process produced a more highly crystalline (23.6%) film. Albeit slightly harder to depolymerize compared to the amorphous counterpart, FAST-PETase was still able to depolymerize these films releasing 23.8 mM of PET monomers at 50 °C in 24 h. Finally, we demonstrate that the complete, non-physically disrupted melted plastic puck from an entire water bottle (roughly 9 g) can be essentially completely degraded by FAST-PETase at 50 °C in less than 2 weeks (Fig. 4d).

Beyond packaging materials, PET is used heavily in the synthetic textile industry. To this end, we evaluated the potential application of FAST-PETase to partially degrade commercial polyester products. Five different commercial polyester products were treated with FAST-PETase at 50 °C, releasing higher amounts of PET monomers relative to that of the samples treated with other PHEs (Fig. 4e). This indicates that FAST-PETase can potentially be used for rapid and efficient degradation of the PET fragments embedded in textile fabrics, providing a potential route for recovering PET monomers from commercial polyester products and reducing the leaching of microfibers into the environment.

Given the high activity of this FAST-PETase mutant at ambient temperatures and pH conditions, we proposed that this enzyme would be suitable for an enzymatic-chemical processing of PET. In this regard, PET depolymerization is only half of the circular plastic economy and we demonstrate here a closed-cycle PET reconstitution by first depolymerizing tinted postconsumer plastic waste using FAST-PETase and subsequently recovering monomers and repolymerizing into virgin PET. TPA was recovered from the degradation solution with a yield of 94.9% and with a purity of over 97% (Supplementary Figs. 9–11). We then regenerate virgin PET directly from the degradation solution using chemical polymerization (Fig. 4f and Supplementary Fig. 12). A complete cycle of degradation to repolymerization can be accomplished in as little as a few days (Supplementary Fig. 13) and demonstrates the feasibility of a closed-loop enzymatic/chemical recycling process to generate a clear, virgin PET film from non-petroleum resources. Moreover, this workflow bypasses the challenges of recycling mixed-colour

PET products. Collectively, these results demonstrate the application of structure-based machine learning for converting mesophilic enzyme scaffolds into broad-range biocatalysts for a cyclic plastic economy.

Online content

Any methods, additional references, Nature Research reporting summaries, source data, extended data, supplementary information, acknowledgements, peer review information; details of author contributions and competing interests; and statements of data and code availability are available at <https://doi.org/10.1038/s41586-022-04599-z>.

- Geyer, R., Jambeck, J. R. & Law, K. L. Production, use, and fate of all plastics ever made. *Sci. Adv.* **3**, e1700782 (2017).
- Santos, R. G., Machovsky-Capuska, G. E. & Andrade, R. Plastic ingestion as an evolutionary trap: toward a holistic understanding. *Science* **373**, 56–60 (2021).
- MacLeod, M., Arp, H. P. H., Tekman, M. B. & Jahnke, A. The global threat from plastic pollution. *Science* **373**, 61–65 (2021).
- Chen, C. C., Dai, L., Ma, L. & Guo, R. T. Enzymatic degradation of plant biomass and synthetic polymers. *Nat. Rev. Chem.* **4**, 114–126 (2020).
- George, N. & Kurian, T. Recent developments in the chemical recycling of postconsumer poly(ethylene terephthalate) waste. *Ind. Eng. Chem. Res.* **53**, 14185–14198 (2014).
- Simon, N. et al. A binding global agreement to address the life cycle of plastics. *Science* **373**, 43–47 (2021).
- Kawai, F., Kawabata, T. & Oda, M. Current knowledge on enzymatic PET degradation and its possible application to waste stream management and other fields. *Appl. Microbiol. Biotechnol.* **103**, 4253–4268 (2019).
- Sarah, K. & Gloria, R. Achieving a circular bioeconomy for plastics. *Science* **373**, 49–50 (2021).
- Ru, J., Huo, Y. & Yang, Y. Microbial degradation and valorization of plastic wastes. *Front. Microbiol.* <https://doi.org/10.3389/fmicb.2020.00442> (2020).
- Ellis, L. D. et al. Chemical and biological catalysis for plastics recycling and upcycling. *Nat. Catal.* **4**, 539–556 (2021).
- Taniguchi, I. et al. Biodegradation of PET: current status and application aspects. *ACS Catal.* <https://doi.org/10.1021/acscatal.8b05171> (2019).
- Tournier, V. et al. An engineered PET depolymerase to break down and recycle plastic bottles. *Nature* **580**, 216–219 (2020).
- Inderthal, H., Tai, S. L. & Harrison, S. T. L. Non-hydrolyzable plastics – an interdisciplinary look at plastic bio-oxidation. *Trends Biotechnol.* **39**, 12–23 (2021).
- Yoshida, S. et al. A bacterium that degrades and assimilates poly(ethylene terephthalate). *Science* **351**, 1196–1199 (2016).
- Chen, C. C. et al. General features to enhance enzymatic activity of poly(ethylene terephthalate) hydrolysis. *Nat. Catal.* <https://doi.org/10.1038/s41929-021-00616-y> (2021).
- Worm, B., Lotze, H. K., Jubinville, I., Wilcox, C. & Jambeck, J. Plastic as a persistent marine pollutant. *Ann. Rev. Env. Resourc.* <https://doi.org/10.1146/annurev-environ-102016-060700> (2017).
- Son, H. F. et al. Rational protein engineering of thermo-stable PETase from *Ideonella sakaiensis* for highly efficient PET degradation. *ACS Catal.* **9**, 3519–3526 (2019).
- Austin, H. P. et al. Characterization and engineering of a plastic-degrading aromatic polyesterase. *Proc. Natl Acad. Sci. USA* **115**, E4350–E4357 (2018).
- Joo, S. et al. Structural insight into molecular mechanism of poly(ethylene terephthalate) degradation. *Nat. Commun.* **9**, 382 (2018).
- Han, X. et al. Structural insight into catalytic mechanism of PET hydrolase. *Nat. Commun.* **8**, 2106 (2017).
- Furukawa, M., Kawakami, N., Oda, K. & Miyamoto, K. Acceleration of enzymatic degradation of poly(ethylene terephthalate) by surface coating with anionic surfactants. *Chem. Sus. Chem.* **11**, 4018–4025 (2018).
- Cui, Y. et al. Computational redesign of a PETase for plastic biodegradation under ambient condition by the GRAPE strategy. *ACS Catal.* <https://doi.org/10.1021/acscatal.0c05126> (2021).
- Chen, K., Hu, Y., Dong, X. & Sun, Y. Molecular insights into the enhanced performance of eklayed petase toward PET degradation. *ACS Catal.* **11**, 7358–7370 (2021).
- Shroff, R. et al. Discovery of novel gain-of-function mutations guided by structure-based deep learning. *ACS Synth. Biol.* **9**, 2927–2935 (2020).
- Kawai, F. et al. A novel Ca^{2+} -activated, thermostabilized polyesterase capable of hydrolyzing polyethylene terephthalate from *Saccharomonospora viridis* AHK190. *Appl. Microbiol. Biotechnol.* **98**, 10053–10064 (2014).
- Weissmann, D. Applied Plastics Engineering Handbook: Processing, Materials, and Applications 2nd edn (ed. Kutz, M.) 717–741 (William Andrew Publishing, 2017).
- Wallace, N. E. et al. The highly crystalline PET found in plastic water bottles does not support the growth of the PETase-producing bacterium *Ideonella sakaiensis*. *Environ. Microbiol. Rep.* **12**, 578–582 (2020).
- Wei, R. & Zimmermann, W. Microbial enzymes for the recycling of recalcitrant petroleum-based plastics: how far are we? *Microb. Biotechnol.* **10**, 1308–1322 (2017).
- Kawai, F., Kawabata, T. & Oda, M. Current state and perspectives related to the polyethylene terephthalate hydrolases available for biorecycling. *ACS Sustain. Chem. Eng.* **8**, 8894–8908 (2020).

Publisher's note Springer Nature remains neutral with regard to jurisdictional claims in published maps and institutional affiliations.

© The Author(s), under exclusive licence to Springer Nature Limited 2022

Article

Methods

CNN model

MutCompute²⁴ is a three-dimensional CNN (3DCNN) model in which the architecture consists of nine layers divided into two blocks: (1) feature extraction and (2) classification. The feature extraction block consisted of six layers: two pairs of 3D convolutional layers followed by a dimension reduction max pooling layer after each pair. The first pair of convolutional layers used filters of size $3 \times 3 \times 3$ and the second pair had filters of size $2 \times 2 \times 2$. For the first pair, the convolutional layers had 100 and 200 filters and for the second pair, the convolutional layers had 200 and 400 filters. Furthermore, the rectified linearity unit function (Relu) was applied to the output of the four convolutional layers. The final feature maps generated by the feature extraction block had dimensions of size $400 \times 3 \times 3 \times 3$. These feature maps were flattened into a one-dimensional vector of size 10,800 before being passed to the classification block. The classification block consisted of three fully connected dense layers given dropout rates of 0.5, 0.2 and 0, respectively. Like the feature extraction block, the output of the first two dense layers was transformed by the Relu function. To obtain a vector of 20 probability scores representing the network prediction for each of the amino acids, we applied a softmax activation function to the output of the third dense layer. MutCompute is available as a machine learning as a service on <https://mutcompute.com>.

MutCompute predictions

MutCompute predictions were obtained by running the WT PETase (PDB ID 5XJH) and ThermoPETase (PDB ID 6IJ6) through our machine learning as a service at <https://mutcompute.com>. Residues were filtered by sorting by the probability assigned to the WT amino acid. We filtered 34 and 39 residues from the WT PETase and ThermoPETase crystal structures, respectively. From these filtered residues, we assigned priority to our experimental mutagenesis by selecting the ten residues from each crystal structure with the highest log₂ fold change between the predicted amino acid and WT amino acid probabilities. Before experimentation, selected residues were visualized with MutCompute-View, which is built on top of NGLViewer (<https://github.com/nglviewer/ngl>), to ensure three things: (1) the prediction was chemically sound and not because of a crystal or model artefact, (2) we were avoiding the active site and binding pocket and (3) avoiding epistatic interactions between predictions and instead targeting predicted ‘instability hot-spots’. MutCompute-View has been made publicly available at <https://mutcompute.com/view>.

Protein crystallization, X-ray diffraction data collection, data processing and model refinement

To identify crystallization conditions for FAST-PETase, a sample containing 6 mg ml⁻¹ purified FAST-PETase was screened in sparse-matrix screening using Phoenix robotic system (Art Robinson). The initial hits were identified with the rod-shaped crystals formed after incubating screening plates at 25 °C for 3 days. The crystallization was optimized as 0.1 M bis-TRIS, 2.0 M ammonium sulfate, pH 5.5 setup as sitting-drop vapour diffusion.

Individual FAST-PETase crystals were flash-frozen directly in liquid nitrogen after cryoprotected with 30% (v/v) glycerol. X-ray diffraction data were collected at the 23-ID-B beamline in the Advance Photon Source. The X-ray diffraction pattern was processed to 1.44 Å resolution for FAST-PETase crystals using HKL2000 (ref. ³⁰). The structure was solved by molecular replacement with ThermoPETase structure as the initial search model (PDB code 6IJ6, ref. ¹⁷). The molecular replacement solution for FAST-PETase structure was iteratively built and refined using Coot³¹ and the Phenix³² refinement package. Procheck and MolProbity evaluated the quality of the finalized FAST-PETase structure. The final statistics for data collection and structural determination are shown in Extended Data Table 1.

Cloning

Genes encoding *I. sakaiensis* 201-F6 /sPETase (WT PETase) (accession number: AOAOK8P6T7), its mutants—PETase^{S121E/D186H/R280A} (ThermoPETase¹⁷) and PETase^{S214H/I168R/W159H/S188Q/R280A/A180I/G165A/Q119Y/L117F/T140D} (DuraPETase²²), cutinase-like enzyme, from *S. AHK190* (ref. ²⁵) (Cut190) (accession number: BAO42836), LCC (accession number: G9BY57) and its mutant LCC^{F243I/D238C/S283C/N246M} (ICCM)¹²—were commercially synthesized for cloning. To enable extracellular expression of PETase and its mutants in *Pseudomonas putida* KT2440 (ATCC 47054), the nucleotide sequence of the signal peptide SP_{put} (21 amino acids) from maltotetraose-forming amylase of *Pseudomonas stutzeri* MO-19 (ref. ³³) was used to substitute the original signal peptide sequence (first 27 amino acids) of WT PETase. The WT PETase and its mutants’ genes with SP_{put} presented at the N terminus were amplified by polymerase chain reaction (PCR) using the synthetic genes as a template. Subsequently, using the Gibson Assembly method, DNA fragments encoding WT PETase, ThermoPETase and DuraPETase were subcloned into a modified pBTK552 vector³⁴ in which the antibiotic resistance marker was swapped from spectinomycin to kanamycin resistance gene and a C-terminal hexa-histidine tag-coding sequence was added. To enable intracellular expression of Cut190, LCC and ICCM in *Escherichia coli* (DE3) (New England Biolabs), the nucleotide sequence encoding the original signal peptide was removed from the synthetic genes. The Cut190, LCC and ICCM genes without signal peptide sequence were amplified by PCR using the synthetic genes as a template. Subsequently, using Gibson Assembly method, the DNA fragments encoding Cut190, LCC and ICCM were subcloned into a commercial vector-pET-21b (Novagen), which carries a C-terminal hexa-histidine tag-coding sequence. The electrocompetent cell *E. coli* DH10β was transformed with the Gibson Assembly product by following a standard electroporation protocol. The resultant expression plasmid DNA was extracted from the overnight culture of the cloning host by using the QIAprep Spin Miniprep kit (Qiagen). The DNA sequence of the extracted plasmid was verified by Sanger sequencing. A list of nucleotide sequences and expressed amino acid sequences of the genes used in the study is provided in Supplementary Methods.

Variant construction

Variants of WT PETase, ThermoPETase and DuraPETase were generated through site-directed mutagenesis using the PCR method described in the Q5 Site-Directed Mutagenesis Kit E0552S (New England Biolabs). The constructed plasmids carrying WT PETase, ThermoPETase and DuraPETase genes were used as the templates for mutagenesis PCR reaction. The corresponding primer sequences and annealing temperature were designed and generated by using the NEBaseChanger tool. Stellar Competent Cells (Clontech Laboratories) were used as the cloning host and transformed with the ligated plasmids using the heat-shock method provided in the manufacturer’s instructions. Plasmid extraction and sequencing for the variants were performed under the same conditions as described for plasmids carrying WT PETase, ThermoPETase and DuraPETase genes.

Protein expression and purification

For extracellular protein expression of WT PETase, ThermoPETase, DuraPETase and their variants, *P. putida* KT2440 was used as the expression host and its electrocompetent cell was transformed with the corresponding constructed plasmids. For intracellular protein expression of Cut190, LCC, ICCM and their variants, *E. coli* BL21 (DE3) was used as the expression host and its electrocompetent cell was transformed with the corresponding constructed plasmids. A single colony of an *P. putida* KT2440 or *E. coli* BL21 (DE3) strain harbouring one of the constructed plasmids was inoculated into 2 ml of Luria Bertani medium with 50 µg ml⁻¹ kanamycin and grown overnight at 37 °C/225 r.p.m. The overnight-grown culture (using 150 µl) was scaled up with 1,000-fold

dilution in a 500-ml triple baffled shake flask and grown to a cell density of 0.8 (optical density (OD_{600}) at 37 °C/225 r.p.m. Protein expression was induced by adding 0.2 mM of isopropyl-β-D-1-thiogalactopyranoside and cells were cultured for 24 h at 30 °C/225 r.p.m. For isolation of the extracellularly expressed PETase enzymes, the induced cell culture was centrifuged at 14,000g and 4 °C for 20 min to obtain the supernatant that accommodates secretory protein. For isolation of the intracellularly expressed Cut190, LCC and ICCM, the induced cell culture was collected by centrifugation at 4,000g and 4 °C for 20 min. Cell pellets were then resuspended in 25 ml of Dulbecco's phosphate buffered saline (DPBS) (Thermo Fisher Scientific) pH 7.0 buffer containing 10 mM imidazole, 1 g l⁻¹ lysozyme and 5 µl of Pierce Universal Nuclease (Thermo Fisher Scientific), followed by mixing on a rocker for 20 min at 4 °C. Subsequently, cells were lysed by sonication and the resulting cell lysate was centrifuged at 14,000g and 4 °C for 20 min to obtain the supernatant that contains soluble proteins. Target proteins from the above two types of supernatant were both purified by HisPur Ni-NTA Resin (Thermo Fisher Scientific) according to the manufacturer's instructions. Desalting of the protein eluent was carried out by using Sephadex G-25 PD-10 columns (GE Healthcare) according to the manufacturer's instructions. All purification and desalting steps were performed at 4 °C in a cold room. Afterwards, the purified protein was concentrated to a final volume of 1 ml by the 50 ml, 10-kDa cut-off Amicon Ultra Centrifugal Filter device (EMD Millipore Corporation) and preserved in DPBS (pH 7.0). The protein concentration was then determined by using the Coomassie Plus Bradford Assay kit (Thermo Fisher Scientific) and the Infinite M200 PRO microplate reader (Tecan) to measure the absorbance of assay mixtures. The presence and purity of the purified proteins were assessed by sodium dodecyl sulfate-polyacrylamide gel electrophoresis.

In vitro analysis of PET-hydrolytic activity using commercial Goodfellow PET film (gf-PET)

To evaluate the PET-hydrolytic activity of PETase and its variants, the homogenous amorphous gf-PET film (Goodfellow, US 577-529-50; specification: 1.3–1.4 g cm⁻³ density, 1.58–1.64 refractive index, 100 × 10⁻¹³ cm³. cm cm⁻² s⁻¹ Pa⁻¹ permeability to water at 25 °C, 20–80 × 10⁻⁶ K⁻¹ coefficient of thermal expansion, 0.13–0.15 W m⁻¹ K⁻¹ at 23 °C thermal conductivity) was used as the substrate for degradation assays with the purified PETase enzyme and its variants. The gf-PET film was prepared in a circular form (6 mm in diameter, roughly 11.4 mg) and was washed three times with 1% SDS, 20% ethanol and deionized water before usage. Subsequently, the gf-PET film was put into a glass test tube and fully submerged in 600 µl of 100 mM KH₂PO₄-NaOH buffer (pH 8.0) with 200 nM purified enzyme. The test tube was tightly capped and wrapped with parafilm to minimize volatilization. The reaction mixture was then incubated at 30, 40, 50, 55 and 60 °C for 96 h. Followed by removing the enzyme-treated gf-PET film from the reaction mixture, the enzyme reaction was terminated by heating at 85 °C for 20 min. The reaction mixture samples were then centrifuged at 10,000g for 5 min. The supernatant of each sample was further analysed by high-performance liquid chromatography (HPLC) for quantifying PET monomers released from the PET depolymerization.

To compare the PET-hydrolytic activity of FAST-PETase with WT PETase, ThermoPETase, DuraPETase, LCC and ICCM across a range of pH (6.5–8.0) at 30 and 40 °C, a similar experimental setup was used. The circular gf-PET film (6 mm diameter, roughly 11.4 mg) was used as the substrate. The enzyme reactions were performed with 200 nM purified enzyme in 600 µl of 100 mM KH₂PO₄-NaOH buffer with various pH values (6.5, 7.0, 7.5 or 8.0) at 30 and 40 °C. After incubating the enzyme reaction for 96 h, the supernatant of the reaction mixture was also analysed by HPLC for quantifying PET monomers released from the PET depolymerization.

Depolymerization of pc-PET plastics

Hole-punched pc-PET films (6 mm in diameter) from 51 postconsumer plastic products were serially treated by 200 nM FAST-PETase in 600 µl

of 100 mM KH₂PO₄-NaOH buffer (pH 8.0) at 50 °C. Fresh enzyme solution was replenished every 22 h to maximize enzymatic depolymerization rate for degrading the 51 samples of various pc-PET films. The supernatant of the enzymatic hydrolysate of the PET samples was analysed by HPLC for quantifying PET monomers released throughout the whole depolymerization process.

The time-course analysis of degrading a pc-PET film (Bean cake container) by various PHEs was conducted at 50 °C. The reactions were performed with 200 nM enzyme in 600 µl of 100 mM KH₂PO₄-NaOH buffer (pH 8.0) and terminated at 6, 12, 18 or 24 h for quantifying total PET monomers released at each time point.

A large, untreated and transparent pc-PET (Bean cake container, roughly 6.4 g) was treated by 200 nM of FAST-PETase in 100 mM of KH₂PO₄-NaOH buffer (pH 8.0) at 50 °C. The whole piece of transparent PET container was fully submerged in 2.5 l of enzyme solution and completely degraded after 48 h.

Depolymerization of an untreated water bottle

To depolymerize an untreated water bottle, fragments were cut out or hole-punched from various sections (finish/neck, shoulder, body, transition to base, base, base centre) of an untreated water bottle (500 ml, CG Roxane LLC.). The fragments were fully submerged in 600 µl of 100 mM KH₂PO₄-NaOH buffer (pH 8.0) with 200 nM purified enzyme. The depolymerization was conducted at 50, 60 and 72 °C for 24 h.

PET water bottle thermal pretreatment

PET water bottles (500 ml, CG Roxane LLC.) were heated at 290 °C on a hot plate covered with aluminium foil. Once PET was melted (about 1 min), another piece of aluminium foil was placed on top of the melted PET. A stainless-steel cylinder (diameter 6 cm, weight 616 g) was used to press the melted PET into a film with a flat surface. After pressing for 1 min, the stainless-steel cylinder was lifted and the PET film was heated again at 290 °C for 15 min. After heating, the hot PET films covered with the aluminium foil was rapidly cooled in an ice bath. After cooling, the reprocessed PET films were peeled off from the aluminium foil.

Meanwhile, a treated but more highly crystalline film can also be produced through a slight modification (after pressing the melted PET films for 1 min by the cylinder, the films were directly quenched by an ice bath without the reheating step) of the above protocol.

Depolymerization of a pretreated water bottle

To depolymerize pretreated water bottle films, circular films (6 mm in diameter; roughly 25 mg) were hole-punched from the pretreated water bottle and treated by 200 nM of various PHEs in 600 µl of 100 mM KH₂PO₄-NaOH buffer (pH 8.0) at temperatures ranging from 50 to 72 °C for 24 h.

To completely depolymerize a pretreated whole water bottle, the melted plastic pucks from an entire water bottle (500 ml; roughly 9 g, CG Roxane LLC.) were cut into small rectangular flakes (roughly 1 × 3 cm). The resulting flakes were then fully submerged in 200 ml of enzyme solution that contained 200 nM of FAST-PETase in 100 mM KH₂PO₄-NaOH buffer (pH 8.0). Depolymerization was conducted at 50 °C and fresh enzyme solution was replenished every 24 h to maximize the enzymatic depolymerization rate.

Depolymerization of polyester products

Five different commercial polyester products were cut into small pieces and used as the substrates that were fully submerged in 600 µl of 100 mM KH₂PO₄-NaOH buffer (pH 8.0) with 200 nM purified enzyme. Enzyme treatment on these five polyester products was conducted at 50 °C. After 24 h of incubation, the reaction was terminated. The enzyme degradation solution was used to determine how much PET monomers were released from hydrolysing these polyester products by various PHEs.

Depolymerization of large, untreated pc-PET container and regeneration of virgin PET

A large, untreated, and green coloured pc-PET container was cut into small rectangular flakes (roughly 1 × 3 cm). Then 3.0 g of the coloured pc-PET flakes was serially treated by 200 nM FAST-PETase in 100 mM KH₂PO₄-NaOH buffer (pH 8.0) at 50 °C. 200 nM of fresh enzyme was added to the degradation solution every 24 h to maximize enzymatic degradation rate. All the coloured pc-PET fragments were completely degraded after 6 days.

On completion of degradation, the enzyme degradation solution was filtered and the filtrate was collected for regeneration. The pH of the filtrate was adjusted to pH 11 with NaOH to hydrolyse remaining MHET. The solution was stirred at room temperature for 4 h to complete the hydrolysis. The pH of the solution was subsequently adjusted to 2 with 37% HCl. The precipitate was filtered and washed several times with deionized water and dried under vacuum overnight. Then 4.3 g of TPA was collected and used in the next step without further purification. Settings used for ¹H nuclear magnetic resonance (NMR) were 400 MHz, d₆-DMSO: 8.03 ppm (s, 4H).

To a suspension of TPA (4.31 g, 25.9 mmol) in CH₃OH (150 ml), 95% H₂SO₄ (2.0 ml) was added dropwise at room temperature. The mixture was stirred at reflux for 24 h and became a clear solution. The reaction mixture was then cooled to room temperature. Dimethyl terephthalate (DMT) was subsequently recrystallized from the reaction mixture and collected after filtration. These white crystals were washed with cold CH₃OH and dried under vacuum for 4 h to afford DMT (4.12 g) with a yield of 82%. ¹H NMR (400 MHz, CDCl₃): 8.08 ppm (s, 4H), 3.93 ppm (s, 6H).

To a three-necked round bottom flask equipped with an air condenser, DMT (4.12 g, 21.1 mmol) was added. The flask was evacuated under vacuum and refilled with nitrogen gas for three times. Ethylene glycol (1.20 ml, 21.5 mmol) was added, followed by the addition of titanium isopropoxide (0.06 ml, 0.21 mmol). The mixture was stirred at 160 °C for 1 h, 200 °C for 1 h and 210 °C for 2 h under nitrogen. The reaction temperature was further increased to 260 °C, and high vacuum was applied to remove unreacted monomers. The mixture was stirred at 260 °C for 2 h and then cooled to room temperature. The resulting PET was dissolved in 1,1,1,3,3-hexafluoro-2-propanol (HFIP, 10 ml) and added dropwise to CH₃OH to remove the catalyst. PET (2.83 g) was collected as white solids after centrifuging and dried under vacuum.

Gravimetric determination of the degraded pc-PET film

The intact pc-PET film was washed three times with 1% SDS, 20% ethanol and deionized water followed by drying the samples under vacuum at 30 °C for 24 h before gravimetric measurement. After enzymatic treatment, the degraded pc-film followed the same washing and drying procedure before gravimetric measurement. The weights of the pc-PET film before and after enzyme treatment were compared to determine the weight loss of the degraded pc-PET film.

Analytical method for measuring PET monomers released

HPLC was used to analyse the PET monomers TPA and MHET released from PET depolymerization. The assay samples were filtered with 0.2-μm nylon syringe filters (Wheaton Science) before running HPLC. Measurement of TPA and MHET was performed using a Dionex Ulti-Mate 3000 (Thermo Fisher Scientific) equipped with an Agilent Eclipse Plus C18 column (3.0 × 150 mm², 3.5 μm) with detection wavelength at 260 nm. Column oven was held at 30 °C with 1% acetic acid in water or 1% acetic acid in acetonitrile as mobile phase over the course of the 30-min sequence under the following conditions: 1 to 5% organic (vol/vol) for 5 min, 5 to 100% organic (vol/vol) for 8 min, 100% organic (vol/vol) for 10 min and 100 to 5% organic for 2 min followed by 5% organic for 5 min. The flow rate was fixed at 0.8 ml min⁻¹. A standard curve was prepared using commercial TPA with ≥99.0% purity (Thermo Fisher Scientific) or MHET ≥97.0% purity (Advanced ChemBlocks Inc.).

Analytical method for measuring melting temperature (*T_m*) of proteins

To evaluate the thermostability of WT PETase and its variants, differential scanning calorimetry (DSC) was used to determine their respective *T_m*. Purified protein samples were concentrated to roughly 300–500 μM using Microcon Centrifugal Filter 10K Devices (Millipore). Then 10 μl of concentrated protein solution (DPBS buffer pH 7.0) was placed in an aluminium Tzero pan and sealed with a Tzero hermetic lid (TA Instruments). *T_m* of the protein samples was analysed by a DSC250 (TA Instruments) with a RCS90 electric chiller. Two DSC procedures were used depending on the anticipated denaturation temperature of the protein. The first DSC method heated from 40 to 90 °C at 10 °C min⁻¹, held at 90 °C for 2 min, then cooled from 90 to 40 °C at -10 °C min⁻¹. The second method heated from 20 to 70 °C at 10 °C min⁻¹, held at 70 °C for 2 min and cooled from 70 to 40 °C at -10 °C min⁻¹. The denaturation temperature of the proteins was measured on the heating ramp trace as the midpoint value at half-height.

Analytical method for determining PET film crystallinity

DSC was used to determine the percentage crystallinity of the PET films hole-punched from the postconsumer plastics. PET film samples (4–10.5 mg) were placed in aluminium Tzero pans with a Tzero solid sample lid. Samples were first heated from 40 to 300 °C at 5 °C min⁻¹, held at 300 °C for 1 min, cooled from 300 to 30 °C at -5 °C min⁻¹ and held at 30 °C for 1 min in a DSC250 (TA Instruments) with a RCS90 electric chiller. The percentage crystallinity was determined on the first heating scan using the enthalpies of melting and cold crystallization. The equation used to calculate percentage crystallinity within the PET film was the following

$$\text{%crystallinity} = \left[\frac{\Delta H_m - \Delta H_{cc}}{\Delta H_m} \right] \times 100$$

where ΔH_m is the enthalpy of melting (J g⁻¹), ΔH_{cc} is the enthalpy of cold crystallization (J g⁻¹), and ΔH_m is the enthalpy of melting for a 100% crystalline PET sample, which is 140.1 J g⁻¹ (refs. ^{12,22}). ΔH_m and ΔH_{cc} were measured by integrating from 90–100 °C to roughly 260 °C with a linear baseline. The percentage crystallinity was calculated using the TRIOS software package. The glass transition temperatures of the PET films were measured using the second heating scan: 30–300 at 10 °C min⁻¹, held at 300 °C for 1 min and then 300–40 °C at -10 °C min⁻¹. The glass transition temperatures for all the PET films were between 80 and 82 °C.

Gel permeation chromatography (GPC)

GPC measurement was performed at an Agilent system with a 1260 Infinity isocratic pump, degasser and thermostated column chamber held at 30 °C. A mixture of chloroform with 50 ppm amylene and 1,1,1,3,3-hexafluoro-2-propanol (2.0 vol%) was used as the mobile phase at 0.5 ml min⁻¹. Molecular weights (Mn, Mw) and polydispersity indices (D) were determined relative to polystyrene standards. For sample preparation for GPC, about 8 mg of PET was dissolved in 0.15 ml 1,1,1,3,3-hexafluoro-2-propanol. Once PET was completely dissolved, chloroform was added to make a total volume of 2.50 ml. The solution was filtered through a polytetrafluoroethylene membrane with a pore size of 0.45 μm. Then 100 μl of the sample solution was injected into the GPC system.

SEM

PET films were mounted onto a 3.2-mm SEM stub using carbon tape. Samples were sputter coated with 8-nm platinum/palladium using a Cressington 208HR Sputter Coater. The metal was sputter coated onto the sample by means of plasma generated with argon present in the chamber. SEM imaging was performed under vacuum using a Zeiss Supra40 SEM. The electron beam intensity was 5 kV.

AFM

AFM was performed on an Aylum MFP-3D atomic force microscope (Asylum Research) in tapping mode. Images were recorded after a surface scan on an area of $50 \times 50 \mu\text{m}^2$. Image analysis, including histograms and surface roughness, was performed using Igor Pro.

NMR spectroscopy

^1H NMR spectroscopy was performed at a 400 MHz Bruker AVANCE NEO spectrometer at room temperature in CDCl_3 or $\text{d}_6\text{-DMSO}$. Chemical shift was referenced to the residual solvent signal (^1H NMR: 7.26 ppm in CDCl_3 , 2.50 ppm in $\text{d}_6\text{-DMSO}$, respectively).

Reporting summary

Further information on research design is available in the Nature Research Reporting Summary linked to this paper.

Data availability

The authors declare that all data supporting the findings of this study are available in the article, its Extended Data, its Source Data or from the corresponding authors upon request. The complete data set of MutCompute predictions used in this study can be acquired at <https://mutcompute.com>. Coordinates for the FAST-PETase structure have been deposited into the PDB with accession code 7SH6. Interactive visualizations of MutCompute for Fig. 1 are available at <https://www.mutcompute.com/petase/5xjh> and <https://www.mutcompute.com/petase/6ij6>. Source data are provided with this paper.

Code availability

MutCompute and MutCompute-View are publicly available at <https://mutcompute.com> and <https://mutcompute.com/view> for academic research.

30. Otwinowski, Z. & Minor, W. Processing of X-ray diffraction data collected in oscillation mode. *Methods Enzymol.* **276**, 307–326 (1997).
31. Emsley, P. & Cowtan, K. Coot: model-building tools for molecular graphics. *Acta Crystallogr. D. Biol. Crystallogr.* **60**, 2126–2132 (2004).

32. Liebschner, D. et al. Macromolecular structure determination using X-rays, neutrons and electrons: recent developments in Phenix. *Acta Crystallogr. Sect. D, Struct. Biol.* **75**, 861–877 (2019).
33. Fujita, M. et al. Cloning and nucleotide sequence of the gene (amyP) for maltotetraose-forming amylase from *Pseudomonas stutzeri* MO-19. *J. Bacteriol.* **171**, 1333–1339 (1989).
34. Leonard, S. P. et al. Genetic engineering of bee gut microbiome bacteria with a toolkit for modular assembly of broad-host-range plasmids. *ACS Synth. Biol.* **7**, 1279–1290 (2018).

Acknowledgements This work was financed under research agreement no. EM10480.26/UTA16-000509 between the ExxonMobil Research and Engineering Company and The University of Texas at Austin. Sequencing was conducted at the Genomic Sequencing and Analysis Facility (RRID no. SCR_021713), SEM was conducted at the Microscopy and Imaging Facility (RRID no. SCR_021756) at the UT Austin Center for Biomedical Research Support, and AFM analysis was conducted at the Texas Materials Institute at UT Austin. N.A.L. and C.Z. thank the Welch Foundation for partial support of this research (Grant #F-1904). The crystallography study is supported by a grant from the National Institutes of Health (no. GM104896 to Y.J.Z.). Crystallographic data collections were conducted at Advanced Photon Sources (BL23-ID-B), Department of Energy national user facility. We acknowledge the Texas Advanced Computing Center at The University of Texas at Austin for providing deep learning resources for neural network predictions and analysis that have contributed to the research results reported in this paper.

Author contributions H.S.A., A.D.E., N.A.L. and H.L. designed and directed the research. In investigation and validation, R.S. and D.J.D. performed neural network analysis. H.L. performed enzyme engineering, purification and the depolymerization experiments of both model and pc-PET substrates. H.L., N.J.C., C.Z., D.J.A. and H.O.C. carried out structural and physical characterization of variants. H.L., C.Z. and N.J.C. performed physical characterization of the treated and untreated commercial PET materials. C.Z. carried out experiments for purifying TPA and regenerating virgin PET and plastics films. D.J.D. and B.R.A. developed MutCompute-View for visualizing predictions from the neural network model. W.K. and Y.J.Z. performed protein crystallization and structural analysis of the engineered enzyme. H.S.A. and H.L. wrote the original draft of the manuscript. H.S.A., A.D.E., N.A.L. and H.L. revised the manuscript. H.S.A. and A.D.E. conceived the project idea. All authors reviewed and accepted the manuscript.

Competing interests A patent has been filed in 2020, ‘Mutations for improving activity and thermostability of PETase enzymes’ relating to the mutants and applications developed in this study. R.S. is a cofounder of Aperiam, a company that applies machine learning to protein engineering. R.S. and A.D.E. are inventors on a patent for applying machine learning to protein engineering that has been licensed to Aperiam.

Additional information

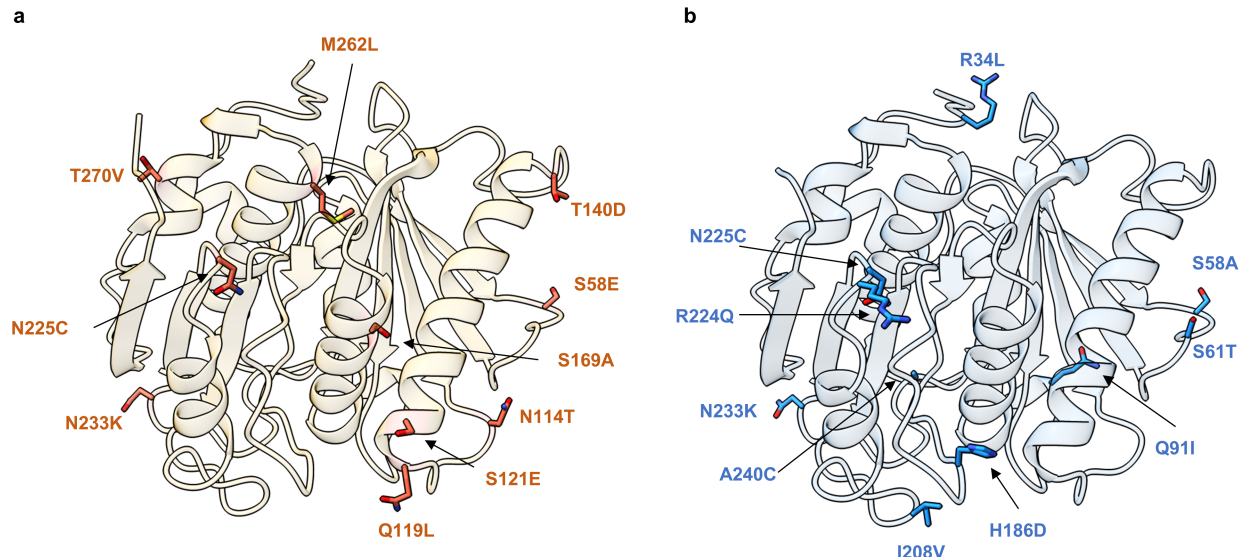
Supplementary information The online version contains supplementary material available at <https://doi.org/10.1038/s41586-022-04599-z>.

Correspondence and requests for materials should be addressed to Hal S. Alper.

Peer review information *Nature* thanks Gregory Bowman, Ulphard Thoden van Velzen and the other, anonymous, reviewer(s) for their contribution to the peer review of this work.

Reprints and permissions information is available at <http://www.nature.com/reprints>.

Article

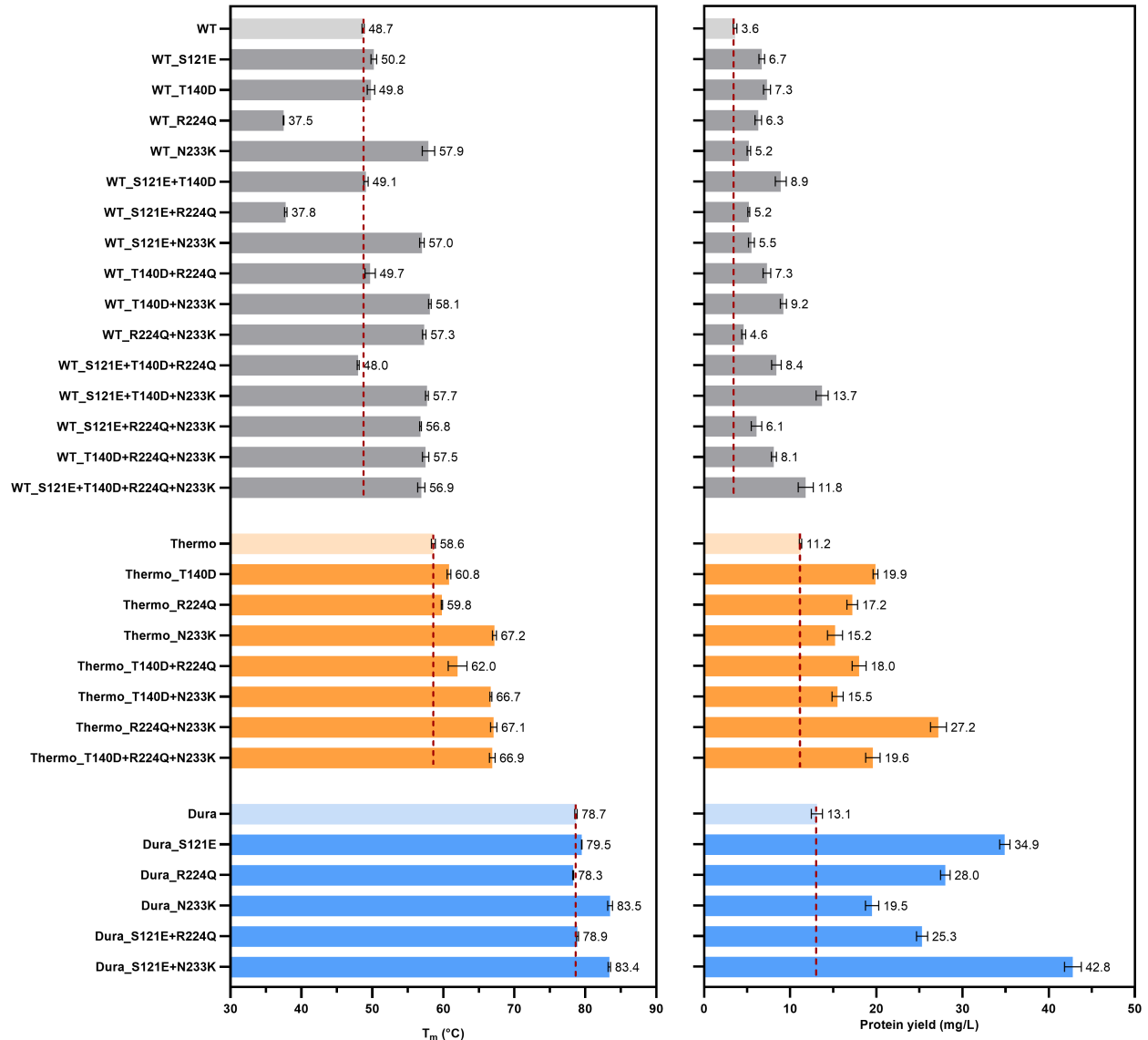


Ranking	Prediction	wt_prob	pred_prob	avg_log_ratio
1	S121E	0.11%	61.20%	6.86
2	M262L	4.12%	66.51%	4.77
3	N233K	4.86%	55.93%	3.06
4	T140D	14.23%	75.20%	2.69
5	S58E	5.22%	45.81%	2.49
6	S169A	10.29%	89.60%	2.46
7	Q119L	6.06%	54.65%	2.40
8	N225C	7.94%	78.08%	2.31
9	T270V	8.65%	72.13%	2.26
10	N114T	9.53%	76.00%	2.14

Ranking	Prediction	wt_prob	pred_prob	avg_log_ratio
1	Q91I	0.09%	98.29%	7.42
2	N233K	0.09%	97.29%	7.39
3	N225C	0.32%	98.01%	5.86
4	S61T	0.54%	31.85%	3.78
5	I208V	3.02%	88.68%	3.57
6	S58A	2.30%	78.28%	3.54
7	R34L	2.99%	78.89%	3.41
8	A240C	9.40%	81.59%	3.24
9	H186D	4.75%	77.21%	3.20
10	R224Q	3.52%	39.61%	3.14

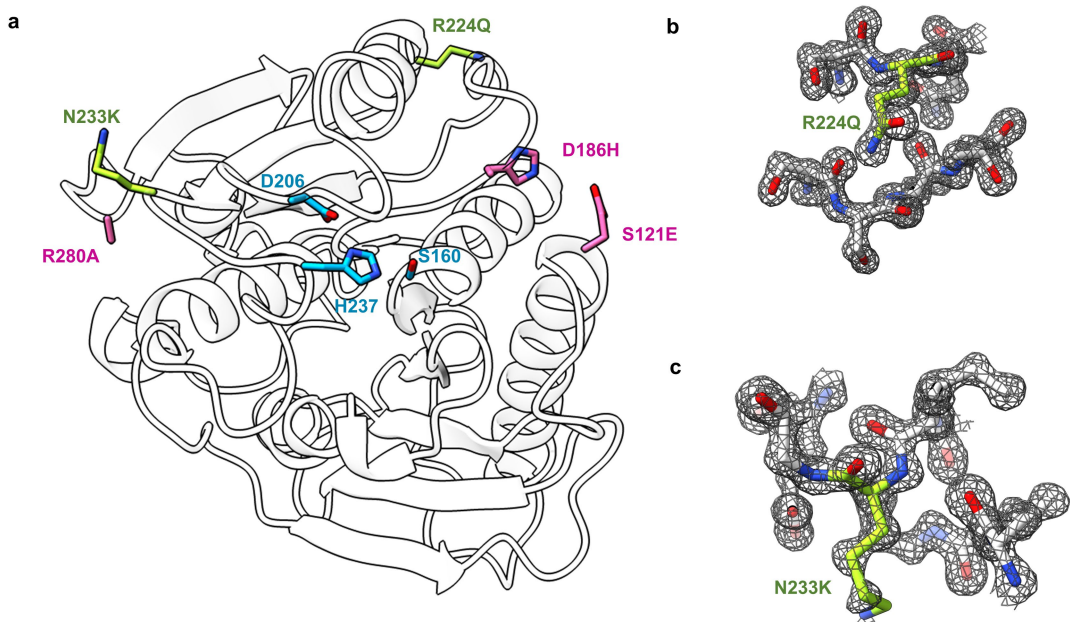
Extended Data Fig. 1 | Top 10 MutCompute predictions ranked by fold change in the probabilities between the predicted and the wild-type amino acid. The top 10 mutations predicted using the wild-type PETase (a) and ThermoPETase (b) as scaffolds are presented. MutCompute is an ensembled model that consist of three individually trained 3-dimensional convolutional

neural network (3DCNN) models. Thus, the avg_log_ratio column is the average of the three log ratio values obtained from the three 3DCNN models, rather than being the log ratio of the average probability assigned to the wild type and predicted amino acid across the three 3DCNN models.



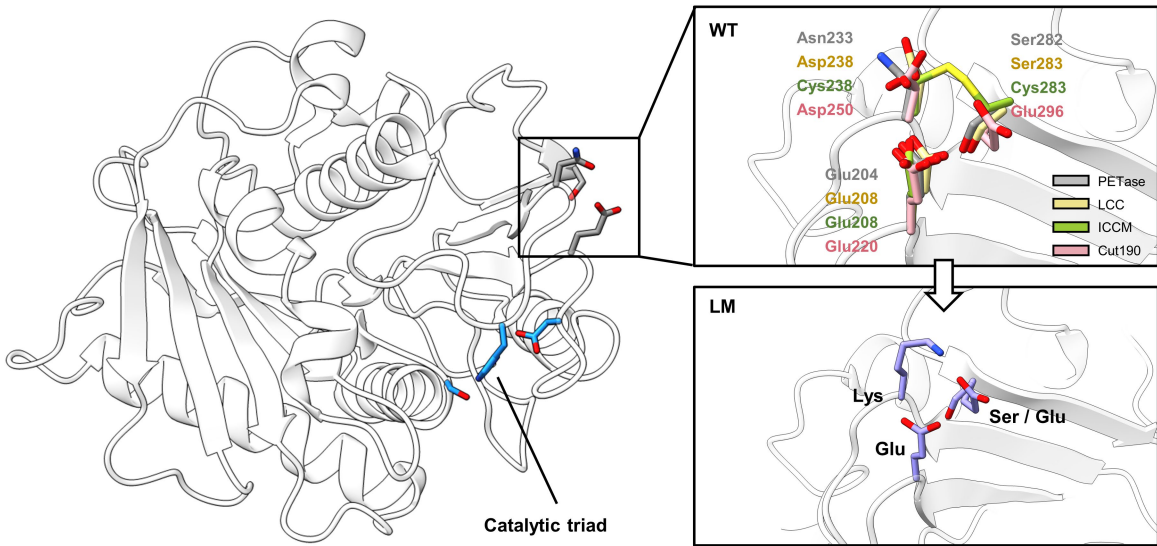
Extended Data Fig. 2 | Thermostability and protein yield of the PETase variants incorporating the predicted mutations and their respective scaffolds—wild-type PETase (WT), ThermoPETase (Thermo), DuraPETase (Dura). T_m of each enzyme (left) was determined by DSC. The protein yield of

each enzyme (right) from *P. putida* purification experiments was evaluated using a Bradford protein assay. All measurements were conducted in triplicate ($n = 3$). The bars shown represent the average numbers.



Extended Data Fig. 3 | X-ray crystal structure of FAST-PETase. **a**, Overall crystal structure of FAST-PETase. Catalytic triads (S160, D206, H237) are shown in blue sticks. Mutations originating from or shared with ThermoPETase (S121E, D186H, R280A) are shown in pink sticks, and completely novel

mutations predicted by MutCompute are shown in green-yellow sticks. **b, c**, 2F_o - F_c map (contoured at 1.5 σ) shown as grey mesh superimposed on the stick models of novel mutation sites (**b**) R224Q, (**c**) N233K.

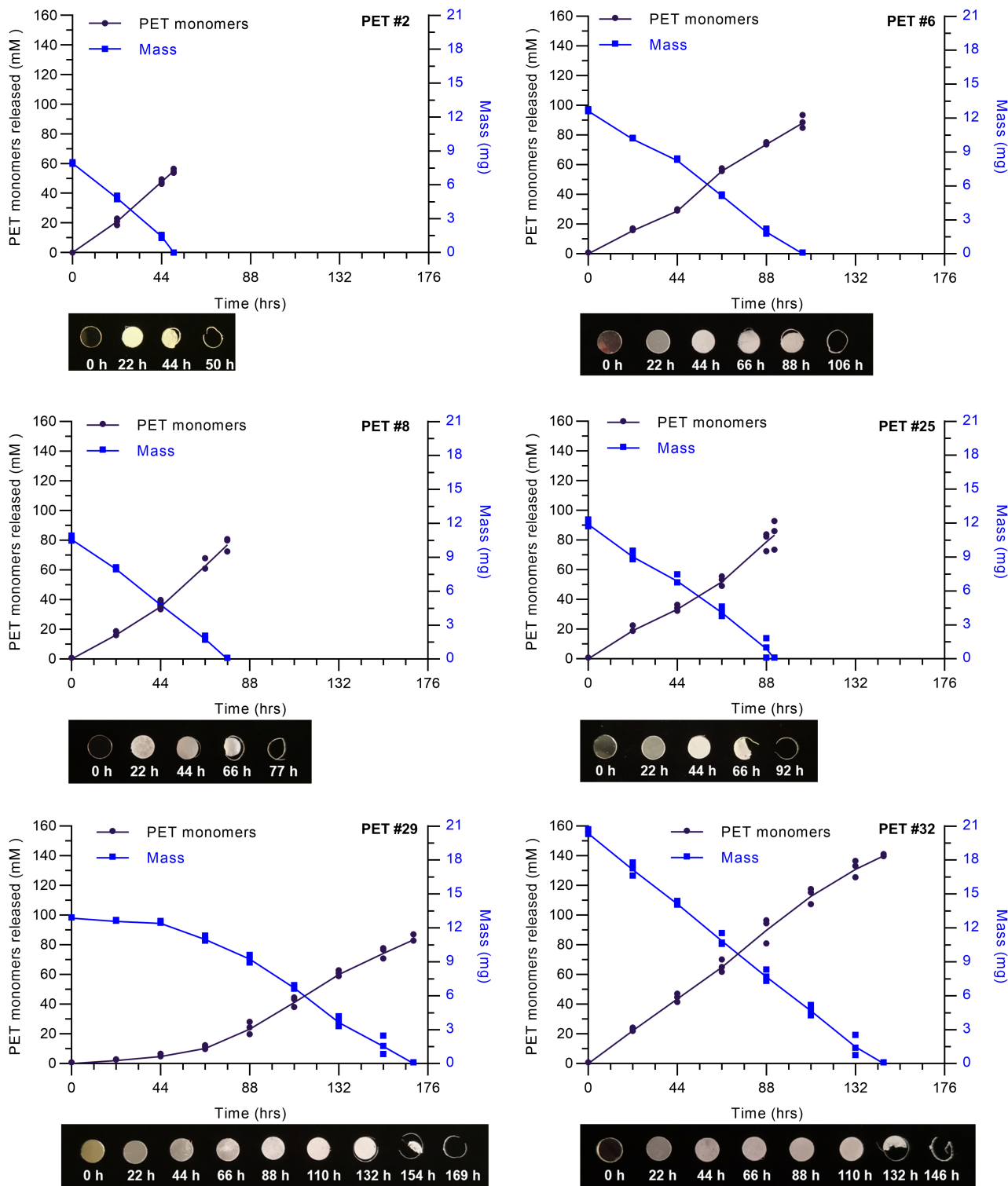


Extended Data Fig. 4 | Location of the LM site in the crystal structures of homologous PHEs.

On wild-type PETase from *I. Sakaiensis* (white ribbon), catalytic residues are shown as blue sticks. LM site is shown as gray sticks on top of cartoon representation. LM site is zoomed in to show superimposed structures of four different homologous PHEs (right top panel: WT): *I. Sakaiensis* wild-type PETase (gray sticks, PDB code 5XJH), LCC (yellow sticks,

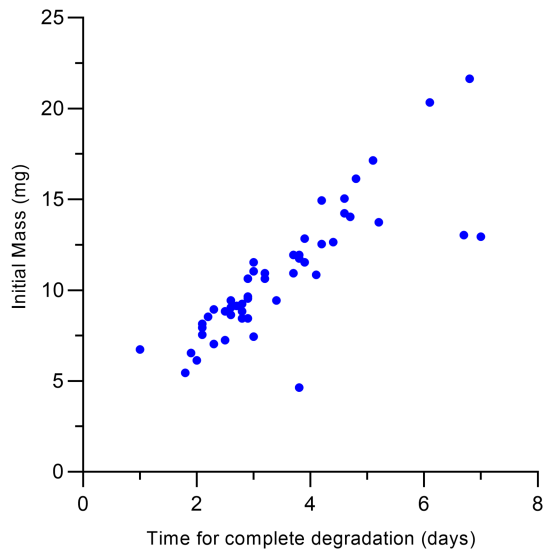
PDB code 4EBO), LCC^{F243I/D238C/S283C/N246M} (ICCM) (green sticks, PDB code 6THT - LCC^{F243I/D238C/S283C/Y127G} (ICCG variant structure), and *S. viridis* Cut190 (pink sticks, PDB code 4WF1 - Cut190^{S226P} variant structure). Based on FAST-PETase structure, the structure of homologous PHEs with LM is modelled (right bottom panel: LM) with residues shown as blue-colored sticks.

Article



Extended Data Fig. 5 | Time-course of mass loss and PET monomers released from hydrolyzing the hole-punched films of six representative pc-PET products with FAST-PETase. The six pc-PET products represent PET #2, 6, 8, 25, 29, 32 that were randomly selected from the 51 pc-PET products (Supplementary Table 3 and Supplementary Fig. 4). The pc-PET films hole-punched from these PET products were hydrolysed by serial treatment

with FAST-PETase at 50 °C until the films were completely degraded (film disappeared). Enzyme solution (200 nM of FAST-PETase in 100 mM KH₂PO₄-NaOH (pH 8.0) buffer) was replenished every 22 h. All measurements were conducted in triplicate ($n = 3$). The squares (mass loss) and circles (PET monomers released) shown represent the individual numbers. The line connects mean values of the timepoints.

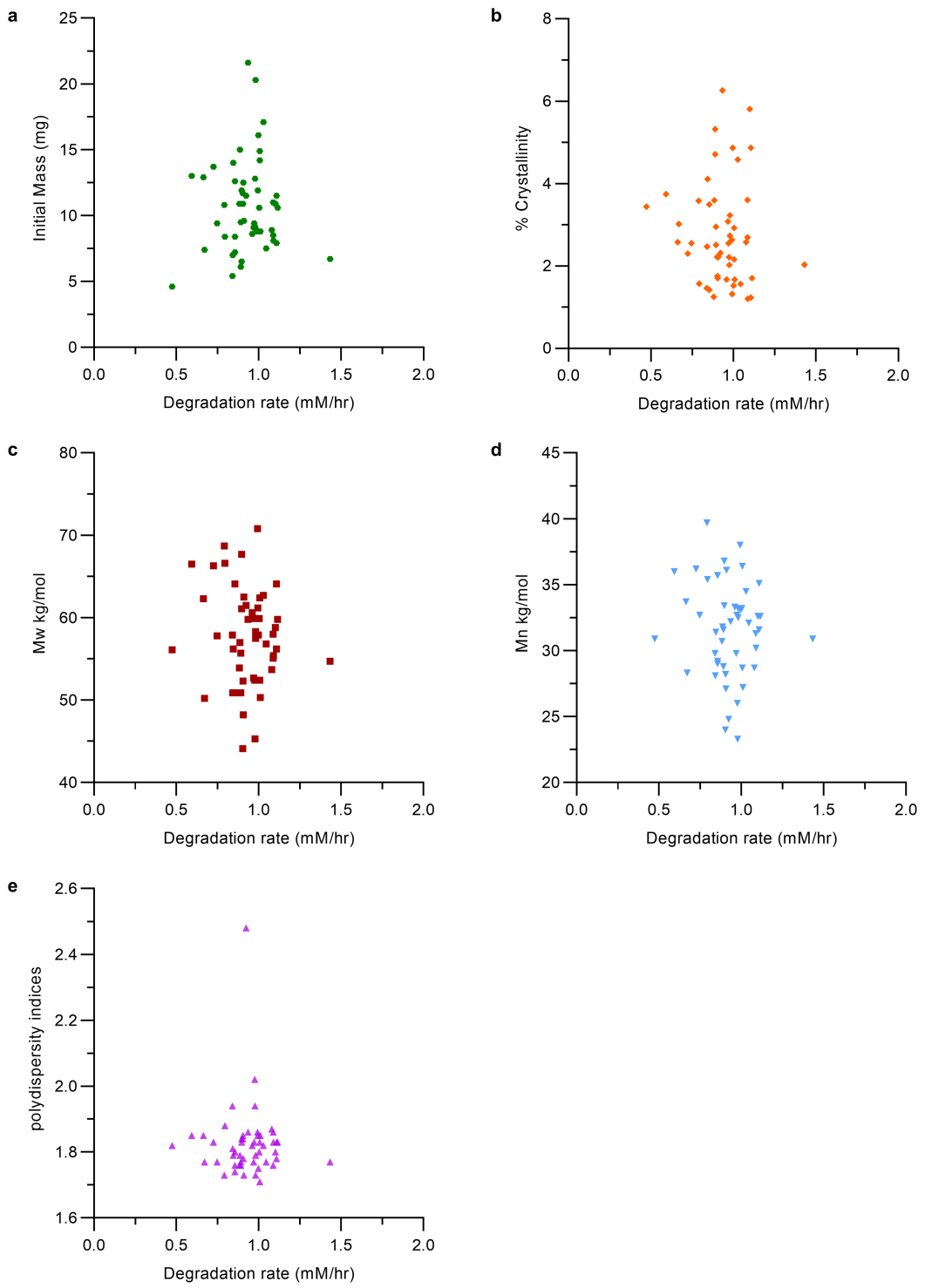


Extended Data Fig. 6 | Scatterplot of time needed for complete degradation

versus initial mass of the hole-punched films from 51 different pc-PET

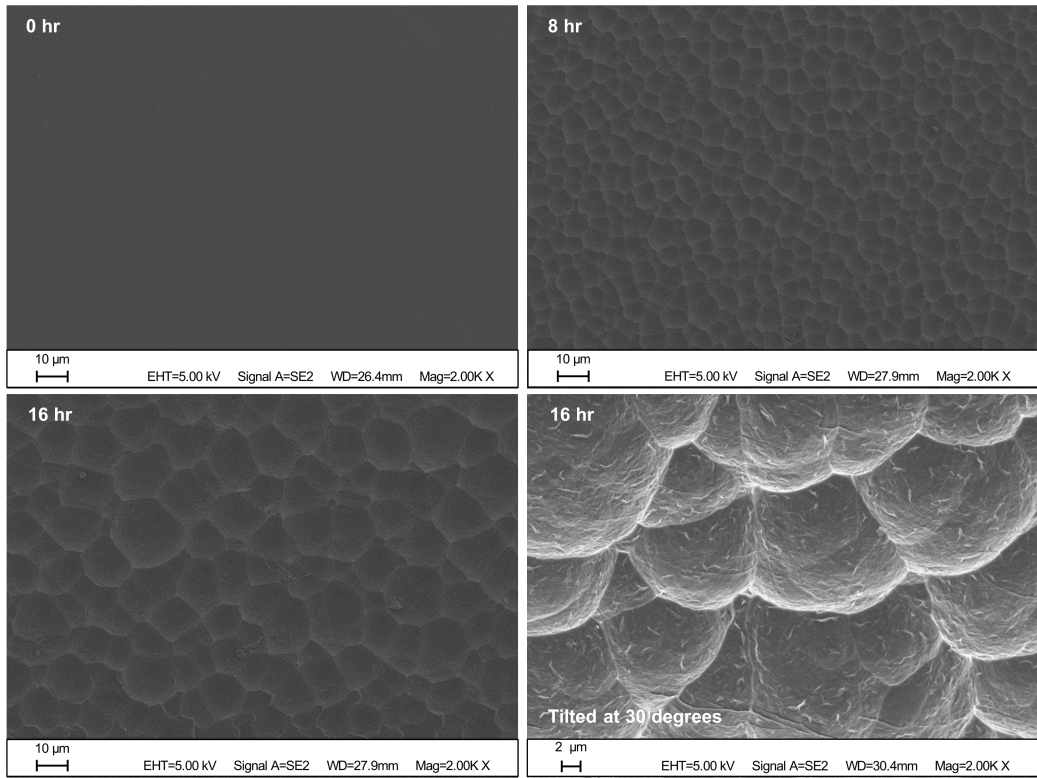
products. Degradation time was found to be correlated with the thickness (as thickness and mass are related) of the hole-punched films from various plastic products.

Article

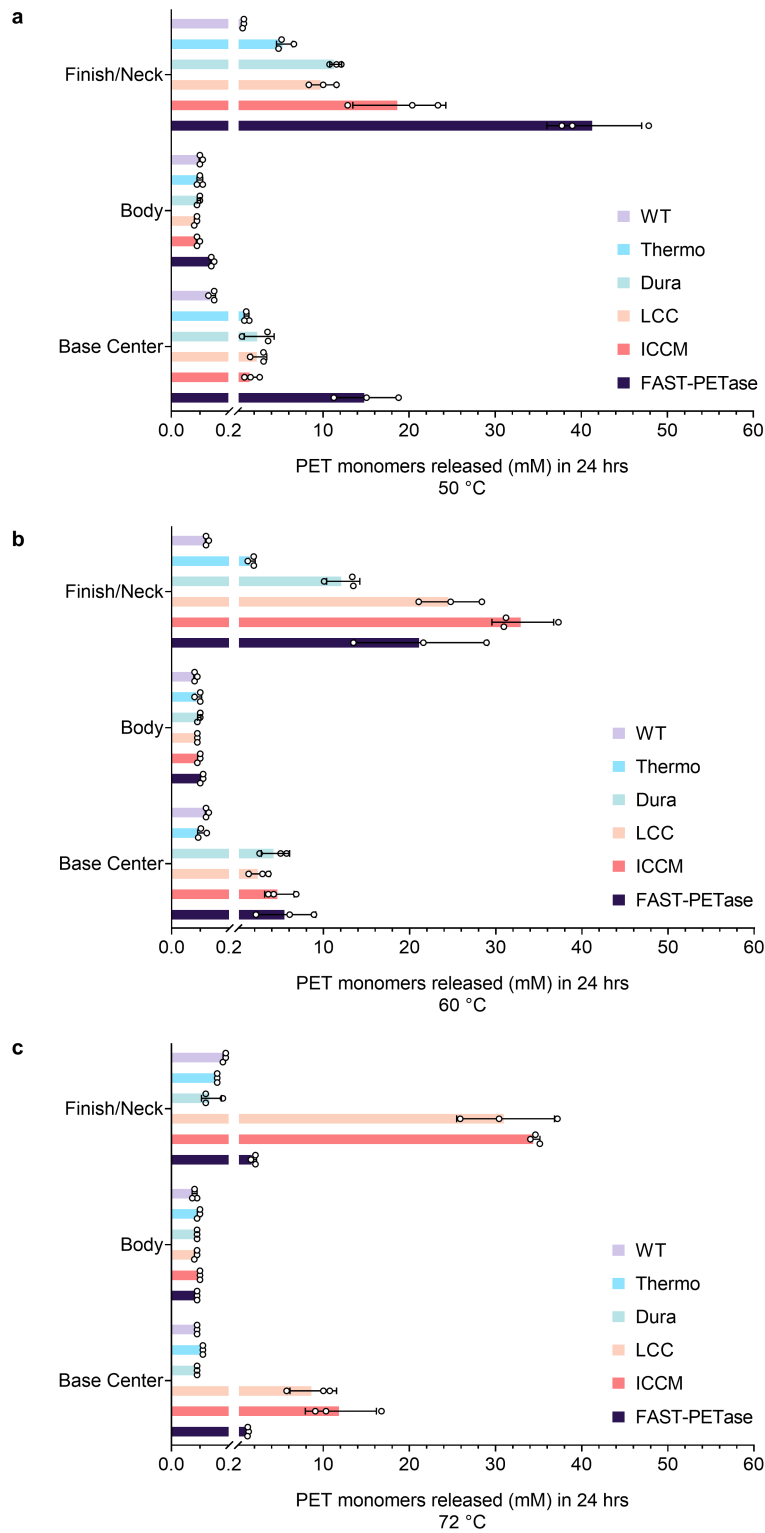


Extended Data Fig. 7 | Scatterplot of degradation rate versus (a.) initial mass, (b.) crystallinity%, (c.) weight average molecular weight (M_w), (d.) number average molecular weight (M_n), or (e.) polydispersity indices of

the hole-punched films from 51 different pc-PET products. Degradation rate was not found to be dependent on any one metric across these various pc-PET plastics.



Extended Data Fig. 8 | Scanning electron microscopic analysis of the pc-PET films. The hole-punched PET films from a bean cake PET container were treated with FAST-PETase for 0 h, 8 h, 16 h in 100 mM KH₂PO₄-NaOH (pH 8.0) buffer at 50 °C.



Extended Data Fig. 9 | Depolymerization of the Finish/Neck, Body and Base Center fragments of an untreated water bottle. Depolymerization was tested by FAST-PETase, wild-type PETase (WT), ThermoPETase (Thermo), DuraPETase (Dura), LCC and ICCM at (a) 50 °C, (b) 60 °C, and (c) 72 °C. All measurements were conducted in triplicate ($n = 3$). The bars and circles shown for each enzyme represent the average and individual numbers, respectively. This comparative analysis provides two main conclusions. First, although higher reaction temperatures do promote the hydrolytic activity of the

thermophilic LCC and ICCM against the amorphous parts of the bottle (base center and finish), the highly crystalline body part still cannot be efficiently depolymerized by any tested enzymes and temperatures. Second, FAST-PETase at 50 °C exhibited the highest overall depolymerization rate seen in these experiments releasing 42, 0.14 and 15 mM of PET monomers within 24 h against the finish, body, and bottom center of the bottle respectively. These values are 25%, 43% and 20% higher, respectively, than that of ICCM at 72 °C.

Extended Data Table 1 | Statistics of the crystal structural determination of FAST-PETase

Data collection	
Space group	P2 ₁ 2 ₁ 2 ₁
Cell dimensions	
a, b, c (Å)	50.9, 51.2, 84.1
α, β, γ (°)	90.0, 90.0, 90.0
Resolution (Å)	50.00-1.44 (1.46-1.44)*
R _{sym} / R _{pim}	0.074(0.195)/0.031(0.113)
CC ½ †	0.988 (0.948)
I / σ	27.4 (3.96)
Completeness (%)	99.4 (94.3)
Redundancy	6.6 (3.5)
Refinement	
Resolution (Å)	43.714 - 1.439 (1.490 - 1.439)
No. reflections	40270 (3753)
R _{work}	0.1515 (0.1641)
R _{free} ‡	0.1657 (0.2118)
No. atoms	2344
Protein	1981
Ligand/ion	5
Water	358
B-factors (Å²)	
Protein	7.8
Ligand/ion	17.6
Water	23.2
R.m.s. deviations	
Bond lengths (Å)	0.012
Bond angles (°)	1.18
Ramachandran plot	
Favored	97.68%
Allowed	2.32%
Outliers	0.00%
Molprobity score	1.16 / 97th percentile

Information about the obtained crystal structure is provided.

Footnote for Extended Data Table 1

*Values for the corresponding parameters in the outermost shell in parenthesis.

†CC_½ is the Pearson correlation coefficient for a random half of the data; the two numbers represent the lowest and highest resolution shell, respectively.

‡R_{free} is the R_{work} calculated for about 10% of the reflections randomly selected and omitted from refinement.

TRIOS

Reporting Summary

Nature Portfolio wishes to improve the reproducibility of the work that we publish. This form provides structure for consistency and transparency in reporting. For further information on Nature Portfolio policies, see our [Editorial Policies](#) and the [Editorial Policy Checklist](#).

Statistics

For all statistical analyses, confirm that the following items are present in the figure legend, table legend, main text, or Methods section.

n/a Confirmed

- The exact sample size (n) for each experimental group/condition, given as a discrete number and unit of measurement
- A statement on whether measurements were taken from distinct samples or whether the same sample was measured repeatedly
- The statistical test(s) used AND whether they are one- or two-sided
Only common tests should be described solely by name; describe more complex techniques in the Methods section.
- A description of all covariates tested
- A description of any assumptions or corrections, such as tests of normality and adjustment for multiple comparisons
- A full description of the statistical parameters including central tendency (e.g. means) or other basic estimates (e.g. regression coefficient) AND variation (e.g. standard deviation) or associated estimates of uncertainty (e.g. confidence intervals)
- For null hypothesis testing, the test statistic (e.g. F , t , r) with confidence intervals, effect sizes, degrees of freedom and P value noted
Give P values as exact values whenever suitable.
- For Bayesian analysis, information on the choice of priors and Markov chain Monte Carlo settings
- For hierarchical and complex designs, identification of the appropriate level for tests and full reporting of outcomes
- Estimates of effect sizes (e.g. Cohen's d , Pearson's r), indicating how they were calculated

Our web collection on [statistics for biologists](#) contains articles on many of the points above.

Software and code

Policy information about [availability of computer code](#)

Data collection

X-ray diffraction data were collected at Advanced Photon Source using beamline 23-ID-B (wavelength 1.03317 Å). Melting temperature (T_m) of PET films and enzymes were determined by Differential scanning calorimetry (DSC). Data were collected using a DSC250 (TA Instruments) with a Trios software (TA Instruments). NMR data were collected at a 400 MHz Bruker AVANCE NEO spectrometer using a Mestrenova software (Mestrelab). Atomic force microscopy (AFM) data were collected using an Asylum MFP-3D atomic force microscope (Asylum Research) using Igor Pro. Scanning electron microscope (SEM) imaging was performed under vacuum using a Zeiss Supra40 SEM. The electron beam intensity was 5 kV. Samples were sputter-coated with 8 nm platinum/palladium using a Cressington 208HR Sputter Coater. Gel permeation chromatography (GPC) was performed at an Agilent system with a 1260 Infinity isocratic pump, degasser, and thermostated column chamber held at 30 °C. Chromoleon software was used for acquisition of spectra on High Performance Liquid Chromatography (HPLC)-Dionex UltiMate 3000 (Thermo Fisher Scientific, Waltham, MA) equipped with an Agilent Eclipse Plus C18 column. The CNN predictions were obtained from mutcompute.com

Data analysis

The X-ray diffraction pattern were processed by using HKL2000.
 The protein crystal structure was solved by molecular replacement with molecular replacement package in Phenix.
 The molecular replacement solution was iteratively built and refined using Coot and Phenix refinement package. Structure analysis and visualization were carried out by Chimera X.
 DSC data were analyzed using a Trios software (TA Instruments).
 NMR data were analyzed using a Mestrenova software (Mestrelab).
 AFM data were analyzed using Igor Pro.
 GPC data were analyzed using Agilent Bio SEC software.
 HPLC data were analyzed using Chromoleon software for integration of chromatograms.
 CNN model predictions were analyzed and processed by the Pandas python package.

For manuscripts utilizing custom algorithms or software that are central to the research but not yet described in published literature, software must be made available to editors and reviewers. We strongly encourage code deposition in a community repository (e.g. GitHub). See the Nature Portfolio [guidelines for submitting code & software](#) for further information.

Data

Policy information about [availability of data](#)

All manuscripts must include a [data availability statement](#). This statement should provide the following information, where applicable:

- Accession codes, unique identifiers, or web links for publicly available datasets
- A description of any restrictions on data availability
- For clinical datasets or third party data, please ensure that the statement adheres to our [policy](#)

Structural coordinates have been deposited into the PDB database.

The mutcompute - view has been added and is publicly accessible at mutcompute.com

Field-specific reporting

Please select the one below that is the best fit for your research. If you are not sure, read the appropriate sections before making your selection.

Life sciences Behavioural & social sciences Ecological, evolutionary & environmental sciences

For a reference copy of the document with all sections, see nature.com/documents/nr-reporting-summary-flat.pdf

Life sciences study design

All studies must disclose on these points even when the disclosure is negative.

Sample size	For enzymatic activity assays, Tm determination, and the experiments incorporating various enzymes and cell, triplicates were performed to determine mean and standard deviation and was stated when relevant. Results are reproducible. Attempts at replication were successful.
Data exclusions	No data was excluded.
Replication	All in vitro and in vivo experiments with explicit standard deviation were performed in triplicates. Attempts at replication were successful.
Randomization	No data was randomized since it was not applicable to our set of experiments.
Blinding	For DSC, SEM, GPC, AFM, HPLC analysis, The analytical team who performed the experiments and analyze the data were blind to the samples that they were handling with and analyzing.

Reporting for specific materials, systems and methods

We require information from authors about some types of materials, experimental systems and methods used in many studies. Here, indicate whether each material, system or method listed is relevant to your study. If you are not sure if a list item applies to your research, read the appropriate section before selecting a response.

Materials & experimental systems

n/a	Involved in the study
<input checked="" type="checkbox"/>	Antibodies
<input checked="" type="checkbox"/>	Eukaryotic cell lines
<input checked="" type="checkbox"/>	Palaeontology and archaeology
<input checked="" type="checkbox"/>	Animals and other organisms
<input checked="" type="checkbox"/>	Human research participants
<input checked="" type="checkbox"/>	Clinical data
<input checked="" type="checkbox"/>	Dual use research of concern

Methods

n/a	Involved in the study
<input checked="" type="checkbox"/>	ChIP-seq
<input checked="" type="checkbox"/>	Flow cytometry
<input checked="" type="checkbox"/>	MRI-based neuroimaging